OCRL1 engages with the F-BAR protein pacsin 2 to promote biogenesis of membrane-trafficking intermediates

Peter G. Billcliff[a,*], Christopher J. Noakes[a,*,†], Zenobia B. Mehta[a,*,‡], Guanhua Yan[a], LokHang Mak[b], Rudiger Woscholski[b], and Martin Lowe[a]
[a]Faculty of Life Sciences, University of Manchester, Manchester M13 9PT, United Kingdom; [b]Department of Chemistry, Imperial College, London SW7 2AZ, United Kingdom

ABSTRACT Mutation of the inositol 5-phosphatase OCRL1 causes Lowe syndrome and Dent-2 disease. Loss of OCRL1 function perturbs several cellular processes, including membrane traffic, but the underlying mechanisms remain poorly defined. Here we show that OCRL1 is part of the membrane-trafficking machinery operating at the *trans*-Golgi network (TGN)/endosome interface. OCRL1 interacts via IPIP27A with the F-BAR protein pacsin 2. OCRL1 and IPIP27A localize to mannose 6-phosphate receptor (MPR)–containing trafficking intermediates, and loss of either protein leads to defective MPR carrier biogenesis at the TGN and endosomes. OCRL1 5-phosphatase activity, which is membrane curvature sensitive, is stimulated by IPIP27A-mediated engagement of OCRL1 with pacsin 2 and promotes scission of MPR-containing carriers. Our data indicate a role for OCRL1, via IPIP27A, in regulating the formation of pacsin 2–dependent trafficking intermediates and reveal a mechanism for coupling PtdIns(4,5)P$_2$ hydrolysis with carrier biogenesis on endomembranes.

INTRODUCTION

Phosphoinositide lipids, of which there are seven species, are important modulators of a wide variety of cellular functions, typically acting to recruit and/or sterically activate downstream effector proteins at distinct cellular locations (Di Paolo and De Camilli, 2006; Balla, 2013). For example, phosphatidylinositol 4,5-bisphosphate (PtdIns(4,5)P$_2$) is abundant at the plasma membrane, where it is a key regulator of endocytosis and actin dynamics. The abundance and spatial distribution of phosphoinositides is tightly controlled by phosphoinositide kinases and phosphatases, which also are highly

regulated (Sasaki *et al.*, 2009). The importance of such regulation is indicated by the fact that numerous human diseases can be attributed to defective phosphoinositide kinase or phosphatase function and the resultant dysregulation of phosphoinositide metabolism that occurs in such cases (McCrea and De Camilli, 2009; Billcliff and Lowe, 2014).

Mutation of the inositol 5-phosphatase OCRL1, whose preferred substrate is PtdIns(4,5)P$_2$, causes two disorders in humans, namely Lowe syndrome and Dent-2 disease (Attree *et al.*, 1992; Hoopes *et al.*, 2005). OCRL1 has been localized to a number of cellular compartments, including clathrin-coated pits, early endosomes, and the *trans*-Golgi network (TGN; Pirruccello and De Camilli, 2012; Mehta *et al.*, 2014). Targeting of OCRL1 depends on binding to Rab GTPases (Hyvola *et al.*, 2006; Hou *et al.*, 2011), with additional partners contributing to the fidelity of membrane recruitment. OCRL1 has been implicated in a number of cellular processes, including endocytic trafficking (Choudhury *et al.*, 2005; Erdmann *et al.*, 2007; Vicinanza *et al.*, 2008; van Rahden *et al.*, 2012; Nandez *et al.*, 2014), cytokinesis (Ben El Kadhi *et al.*, 2011; Dambournet *et al.*, 2011), ciliogenesis (Coon *et al.*, 2012; Luo *et al.*, 2012; Rbaibi *et al.*, 2012), cell junction formation (Grieve *et al.*, 2011), and cell migration (Coon *et al.*, 2009). How OCRL dysfunction can affect so many processes is unclear (Mehta *et al.*, 2014). In some cases, OCRL1 appears to act directly—for example in clathrin vesicle formation at the plasma membrane. However, whether this is true for most of the cellular

Abbreviations used: BAR, Bin–Amphiphysin–Rvs; CIMPR, cation-independent mannose 6-phosphate receptor; EHD, epsin homology domain; IPIP27, inositol phosphatase interacting protein of 27 kDa; OCRL1, oculocerebrorenal syndrome of Lowe 1; SH3, Src homology 3; SNX1, sorting nexin 1; TGN, *trans*-Golgi network.

defects observed upon OCRL1 loss or instead reflects a more general role for OCRL1 in maintaining PtdIns(4,5)P$_2$ homeostasis is not clear.

The PH domain proteins IPIP27A and B (also known as Ses1 and 2) have been identified as novel interactors of OCRL1 (Swan et al., 2010; Noakes et al., 2011). We previously showed that the IPIP27 proteins are required for efficient endocytic recycling (Noakes et al., 2011). Here we demonstrate that IPIP27A can physically link OCRL1 to the F-BAR–domain protein, protein kinase C and casein kinase 2 substrate in neurons (pacsin) 2 (also known as syndapin 2; Kessels and Qualmann, 2004). Pacsin 2 is part of the trafficking machinery, able to sculpt membranes through its F-BAR domain and interactions with the actin cytoskeleton, as well as coordinate carrier morphogenesis with membrane scission through interactions with dynamin and/or eps15 homology domain–containing (EHD) proteins (Kessels and Qualmann, 2004; Kostan et al., 2014; Quan and Robinson, 2014). Our findings indicate that OCRL1 and IPIP27A function together with pacsin 2 to regulate formation of trafficking intermediates containing the mannose 6-phosphate receptor (MPR) at the TGN and endosomes and suggest an important role for PtdIns(4,5)P$_2$ hydrolysis in regulating this process.

RESULTS

IPIP27A links pacsin 2 to OCRL1

We previously proposed that the IPIP27 proteins act as adaptors, linking OCRL1 to machinery involved in endocytic trafficking (Noakes et al., 2011). To explore this possibility, we performed pull-down experiments using a HeLa cell extract and C-terminal fragments of IPIP27A and IPIP27B as bait, with bound proteins identified by mass spectrometry. Using this approach, we identified the actin-associated SH3 domain proteins myosin 1E, pacsin 2, and CD2AP as partners for IPIP27A but not IPIP27B (Supplemental Figure S1). We decided to focus on pacsin 2 for further study, which has an F-BAR domain (Figure 1A), due to its role in biogenesis of trafficking intermediates (Kessels and Qualmann, 2004; Kostan et al., 2014; Quan and Robinson, 2014). Binding of pacsin 2 to IPIP27A was confirmed by Western blotting (Figure 1B, bottom). Note that pacsin 2 binds only to IPIP27A, whereas OCRL1 binds to both IPIPs, as reported previously (Swan et al., 2010; Noakes et al., 2011; Supplemental Figure S1 and Figure 1B, top). Similar results were obtained using green fluorescent protein (GFP)–tagged pacsin 2 transiently expressed in HeLa cells (Figure 1C). IPIP27A has several PxxP motifs in its C-terminal region that are potential SH3 domain–binding sites (Figure 1A). We therefore reasoned that IPIP27A would bind to the SH3 domain of pacsin 2. This was the case, because the SH3 domain of pacsin 2 was sufficient for IPIP27A binding (Figure 1D, rightmost column), and binding was abolished by mutation of a conserved proline residue in the peptide-binding groove of the SH3 domain (P478L) (Figure 1, A and C, bottom). No binding of IPIP27A to the SH3 domain proteins cortactin, signal-transducing adapter molecule, and sorting nexin 9 (SNX9), which was recently shown to bind directly to OCRL1 (Nandez et al., 2014), was observed, indicating that IPIP27A binding to SH3 domain proteins is selective (Figure 1C).

Mutation of the various PxxP motifs in IPIP27A revealed that a ^{203}PPPxPPRR^{210} motif located upstream of the 5-phosphatase binding F&H motif is the major pacsin 2 binding site (Figure 1, A and D). Mutation of the Pro residues or the pair of C-terminal Arg residues in this motif almost completely abolished pacsin 2 binding, whereas mutation of another putative PxxP motif in the C-terminal region of IPIP27A (^{215}PHGP^{218}) had no effect on binding (Figure 1D, bottom). Given the similarity between the SH3 domains of the different human pacsins, we next tested whether IPIP27A can bind to pacsin 1, which

is neuronal specific, and pacsin 3, which has a more restricted tissue expression than the ubiquitous pacsin 2 (Kessels and Qualmann, 2004). IPIP27A is able to interact with all pacsins (Supplemental Figure S2A), suggesting that it likely participates more widely in pacsin function. IPIP27 and pacsin 2 can be coimmunoprecipitated from cell extracts, consistent with interaction in vivo (Figure 1E).

To determine whether IPIP27A can physically link pacsin 2 to OCRL1, we performed in vitro binding experiments with recombinant proteins. When GST-IPIP27A C-terminus was coupled to beads and incubated with purified OCRL1 in the presence of increasing amounts of maltose binding protein (MBP)–tagged pacsin 2 SH3 domain, both ligands simultaneously bound to IPIP27A, with pacsin 2 binding increasing in proportion to the amount added (Figure 1F). This is consistent with the binding of pacsin 2 and OCRL1 to distinct sites in IPIP27A. Of interest, OCRL1 contains a PxxP motif in the N-terminal region (^{175}REPPPPP^{181}) that was previously shown to bind SNX9 (Nandez et al., 2014), raising the possibility of OCRL1 binding directly to the SH3 domain of pacsin 2. However, we could rule this out by showing that OCRL1 is unable to bind pacsin 2 in the absence of IPIP27A (Supplemental Figure S2B). Taken together, these results indicate that IPIP27A can physically link pacsin 2 to OCRL1 through distinct binding sites in its C-terminal region.

Pacsin 2 colocalizes with OCRL1 and IPIP27A at the TGN and early endosomes

Previous work has shown that although pacsin 2 is predominantly diffuse in the cytoplasm, pools of the protein reside at various compartments, including the TGN and endosomes (Kessels et al., 2006; de Kreuk et al., 2011; 2012; Giridharan et al., 2013). We therefore examined whether pacsin 2 colocalizes with OCRL1 and IPIP27A on these compartments. For this purpose, we expressed tagged versions of the proteins at low levels in COS-7 cells and visualized them by fluorescence microscopy. As shown in Figure 2A, we confirmed colocalization of GFP–pacsin 2 with mCherry-OCRL1 and Myc-IPIP27A at both early/recycling endosomes, marked with EEA1 and transferrin receptor, and the TGN, marked with golgin-97. Endogenous pacsin 2, detected with a custom-made antibody, was similarly localized (Figure 2B). Quantification revealed that 69% (n = 470) of OCRL1-positive compartments contained pacsin 2, with a high degree of colocalization between OCRL1 and pacsin 2, indicated by a Pearson's r = 0.78 ± 0.10 (SD, n = 64). Of interest, when we expressed the D40K mutant of pacsin 2, which has increased membrane binding and tubulation properties (Shimada et al., 2010), we observed increased recruitment of OCRL1 onto pacsin 2–positive cytoplasmic puncta and tubules in the presence but not absence of ectopically expressed IPIP27A (Figure 2C). Recruitment was abolished using IPIP27A mutants unable to bind OCRL1 (F224A) or pacsin 2 (RR > AA), confirming that interactions with both proteins are required for the observed recruitment (Figure 2C). This result indicates that IPIP27A can physically link OCRL1 to membrane-associated pacsin 2 in vivo, consistent with the formation of a tripartite complex in cells.

OCRL1 and IPIP27A are present on TGN and endosome-derived cation-independent MPR trafficking intermediates

The ability of IPIP27A to physically link OCRL1 with pacsin 2, a protein involved in the biogenesis of trafficking intermediates, implies a direct role for OCRL1 in the carrier formation process. A recent study showed that OCRL1 functions at a late stage of clathrin-coated vesicle formation at the plasma membrane (Nandez et al., 2014). However, it remains to be determined whether OCRL1 or
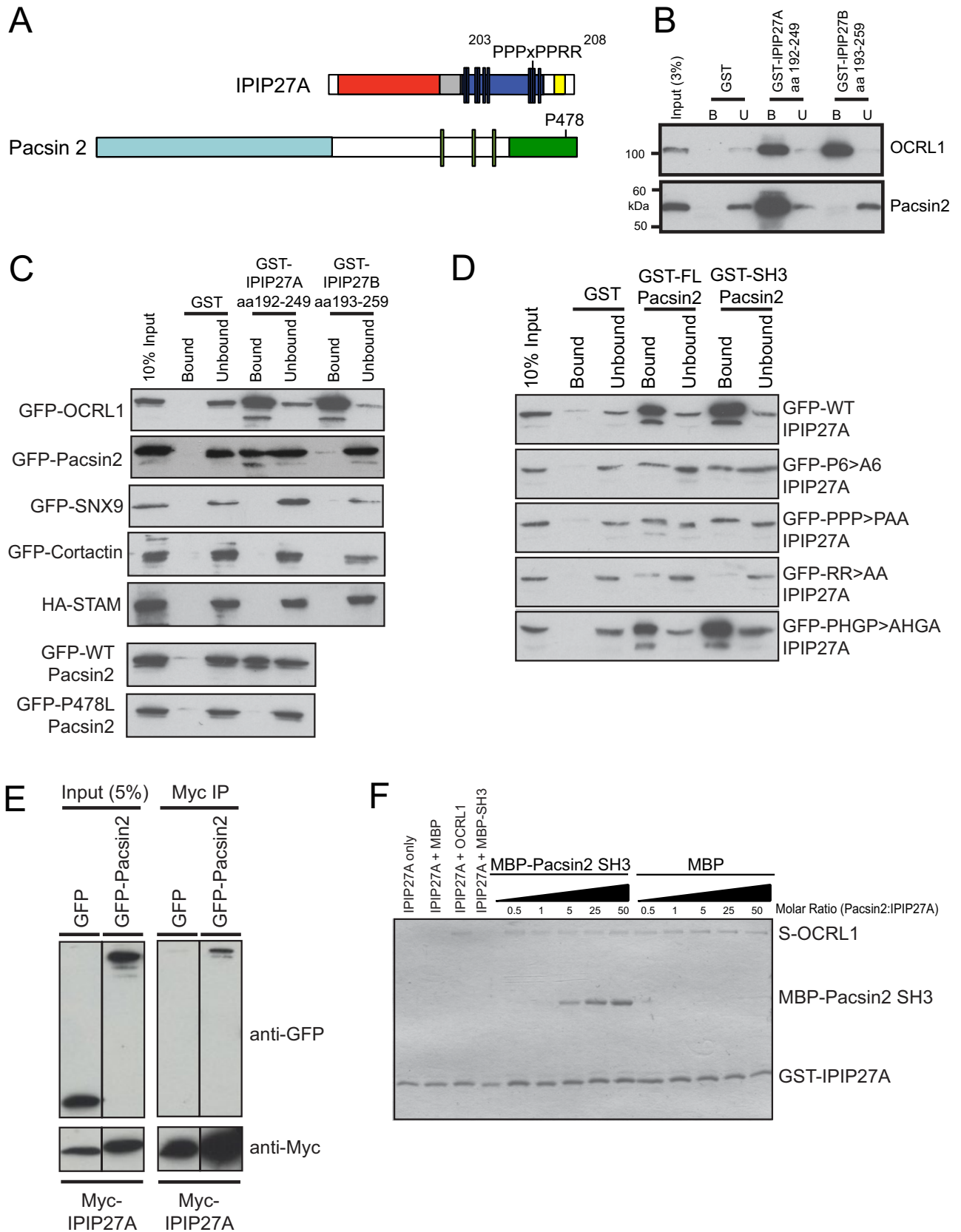
FIGURE 1: Interaction of IPIP27A with pacsin 2. (A) Schematic view of IPIP27A and pacsin 2. IPIP27A contains an N-terminal PH domain (red), a coiled-coil region (gray), a proline-rich region (navy blue), and a C-terminal F&H motif that mediates binding to OCRL1 and INPP5B (yellow). Vertical bars correspond to putative PxxP motifs. The 203PPPxPPRR210 motif is highlighted. Pacsin 2 has an N-terminal F-BAR domain (light blue) and a C-terminal SH3 domain (green). The green vertical bars correspond to NPF motifs that mediate binding to EHD proteins. (B) Beads

IPIP27A functions in biogenesis of trafficking intermediates at endomembranes. MPR trafficking at the TGN/endosome interface is sensitive to loss of either protein, raising the possibility that they may function in biogenesis of cation-independent MPR (CIMPR)–containing carriers at the TGN or endosomes (Choudhury et al., 2005; Hyvola et al., 2006; Cui et al., 2010; Noakes et al., 2011; Vicinanza et al., 2011; van Rahden et al., 2012). We therefore examined whether OCRL1 or IPIP27A associates with MPR trafficking intermediates forming at the TGN and early endosomes. For this purpose, we transiently expressed mCherry-OCRL1 or IPIP27A in COS-7 cells stably expressing low levels of GFP-CIMPR and performed spinning-disk confocal time-lapse microscopy. There was extensive colocalization of GFP-CIMPR with mCherry-OCRL1 in both the perinuclear TGN and more peripheral endosomes (Figure 3A and Supplemental Figure S3). Rapid time-lapse imaging under these conditions indicates the presence of OCRL1 in CIMPR-containing structures, most likely corresponding to trafficking intermediates, budding from larger TGN and endosomal compartments (Figure 3A and Supplemental Videos S1 and S2). The budding structures sometimes appeared as short tubules or were more vesicular in nature, and after detachment they moved away from the donor compartment. Time-lapse imaging revealed that mCherry-IPIP27A was also present on CIMPR- and OCRL1-positive carriers (Figure 3B and Supplemental Video S3).

We next analyzed whether OCRL1 is present on other carriers that bud from early endosomes. Covisualization of mCherry-OCRL1 with GFP-transferrin receptor (TfR), which is packaged into carriers destined for the plasma membrane or recycling endosomes (Maxfield and McGraw, 2004), revealed that TfR-containing tubular carriers are devoid of OCRL1 (Supplemental Figure S4A). We also analyzed Wls, which is trafficked in a retromer- and sorting nexin 3–dependent manner from endosomes to the TGN (Harterink et al., 2011). OCRL1 was also absent from Wls containing tubular carriers emerging from endosomes (Supplemental Figure S4B).

Previous studies showed that the retromer-associated BAR domain protein SNX1 functions in endosome-to-TGN trafficking of CIMPR, where it contributes to the biogenesis of trafficking intermediates (Arighi et al., 2004; Carlton et al., 2004; Seaman, 2004). To determine whether the endosome-derived OCRL1-positive carriers also contain SNX1 or represent a distinct type of carrier, we covisualized GFP-tagged SNX1 and mCherry-OCRL1 by time-lapse microscopy. As expected from previous work (Carlton et al., 2004), GFP-SNX1 was present on tubular carriers emanating from endosomes (Figure 3C and Supplemental Videos S4 and S5). Although OCRL1 was present on the same parental endosomes as SNX1, it was absent from the SNX1 carriers (Figure 3C and Supplemental Videos S4 and S5). These results indicate that the OCRL1- and IPIP27A-containing CIMPR carriers are distinct from those that contain SNX1 and vice versa.

IPIP27A functions with pacsin 2 in CIMPR carrier biogenesis

We next investigated whether IPIP27A, which links OCRL1 to pacsin 2, is required for the formation of CIMPR-containing trafficking intermediates. IPIP27A was depleted using RNA interference (RNAi; Figure 4A), and CIMPR trafficking was analyzed by time-lapse microscopy. As expected, in control cells, GFP-CIMPR was abundant in the perinuclear TGN and more peripheral endosomes and dynamic carriers moving between these compartments (Figure 4, B and E). The budding of vesicular and short tubular carriers was frequently observed, as previously reported (Waguri et al., 2003; Anitei et al., 2010; Temkin et al., 2011; Figure 4E and Supplemental Videos S6 and S7). Strikingly, in IPIP27A-depleted cells, the detachment of GFP-CIMPR carriers was impaired, and they appeared as elongated tubules emanating from both the perinuclear TGN and peripheral endosomes (Figure 4, B and E, and Supplemental Videos S8–S10). Both the number of CIMPR tubules and their length were dramatically increased upon IPIP27A depletion (Figure 4, C and D). Some of the tubules were long-lived, although most were dynamic and grew or collapsed during the course of the movies (Figure 4E and Supplemental Videos S8–S10). The impaired detachment of the CIMPR tubules from the donor membrane is suggestive of a membrane scission defect. The phenotype was observed with two independent small interfering RNAs (siRNAs) and also to a lesser extent in a genome-edited HeLa line lacking IPIP27A, confirming its specificity (Supplemental Figure S5, A and B). Depletion of IPIP27A also elicited a similar phenotype in COS-7 cells (Supplemental Figure S5C).

To determine whether pacsin 2 is required for generation of the CIMPR tubules in IPIP27A-depleted cells, we depleted it alone or together with IPIP27A and imaged GFP-CIMPR dynamics in live cells. As shown in Figure 4, F–H, pacsin 2 depletion caused a marked reduction in both the abundance and length of GFP-CIMPR tubules, indicating a requirement for pacsin 2 in forming these structures. To confirm the specificity of the tubulation phenotype, we examined whether depletion of the endosomal BAR domain protein SNX1 would cause a similar effect. As shown in Figure 4I, depleting SNX1 did not affect the CIMPR tubulation elicited by IPIP27A depletion. Neither tubule abundance nor tubule length was affected by SNX1 depletion (Figure 4, J and K). Conversely, depletion of either IPIP27A or pacsin 2 had no effect on SNX1 carrier formation (Supplemental Figure S6). Taken together, these results indicate aberrant formation of pacsin 2–dependent CIMPR carriers upon loss of IPIP27A and that these carriers are functionally distinct from those containing SNX1.

We next sought to confirm the functional importance of interactions between pacsin 2, IPIP27A, and OCRL1. Unfortunately we were unable to rescue the tubulation phenotype by reexpression of wild-type IPIP27A, precluding rescue experiments with binding mutants. We attribute this to an inability to achieve uniform expression of IPIP27A at endogenous or close to endogenous levels. We therefore resorted to an overexpression strategy. We previously showed that expression of OCRL1 lacking the catalytic domain (OCRL1ΔPIP2)

with the indicated GST-tagged proteins as bait were incubated with HeLa cell extract, and bound OCRL1 and pacsin 2 were detected by Western blotting. (C) Extracts of HeLa cells expressing the indicated tagged proteins were incubated with beads containing GST-tagged bait proteins and binding assessed by Western blotting with anti-GFP or anti-HA antibodies. (D) GST-tagged bait proteins were incubated with extracts from HeLa cells expressing GFP-tagged wild-type (WT) IPIP27A or the indicated point mutants (203PPPPPP208>AAAAAA, designated as P6>A6, 203PPP205>PAA, 209RR210>AA, all in the 203PPPxPPRR210 motif; and 215PHGP218>AHGA, outside the motif), and binding was assessed by Western blotting with anti-GFP antibodies. (E) HeLa cells coexpressing Myc-IPIP27A and either GFP or GFP-pacsin 2 were subjected to coimmunoprecipitation with anti-Myc antibodies and analysis by Western blotting with anti-Myc and anti-GFP antibodies. (F) Beads containing GST-IPIP27A C-terminal fragment were incubated in the absence or presence of S-tagged OCRL1 with increasing concentrations of MBP or MBP-pacsin 2 SH3 domain as indicated and binding analyzed by Coomassie blue staining.
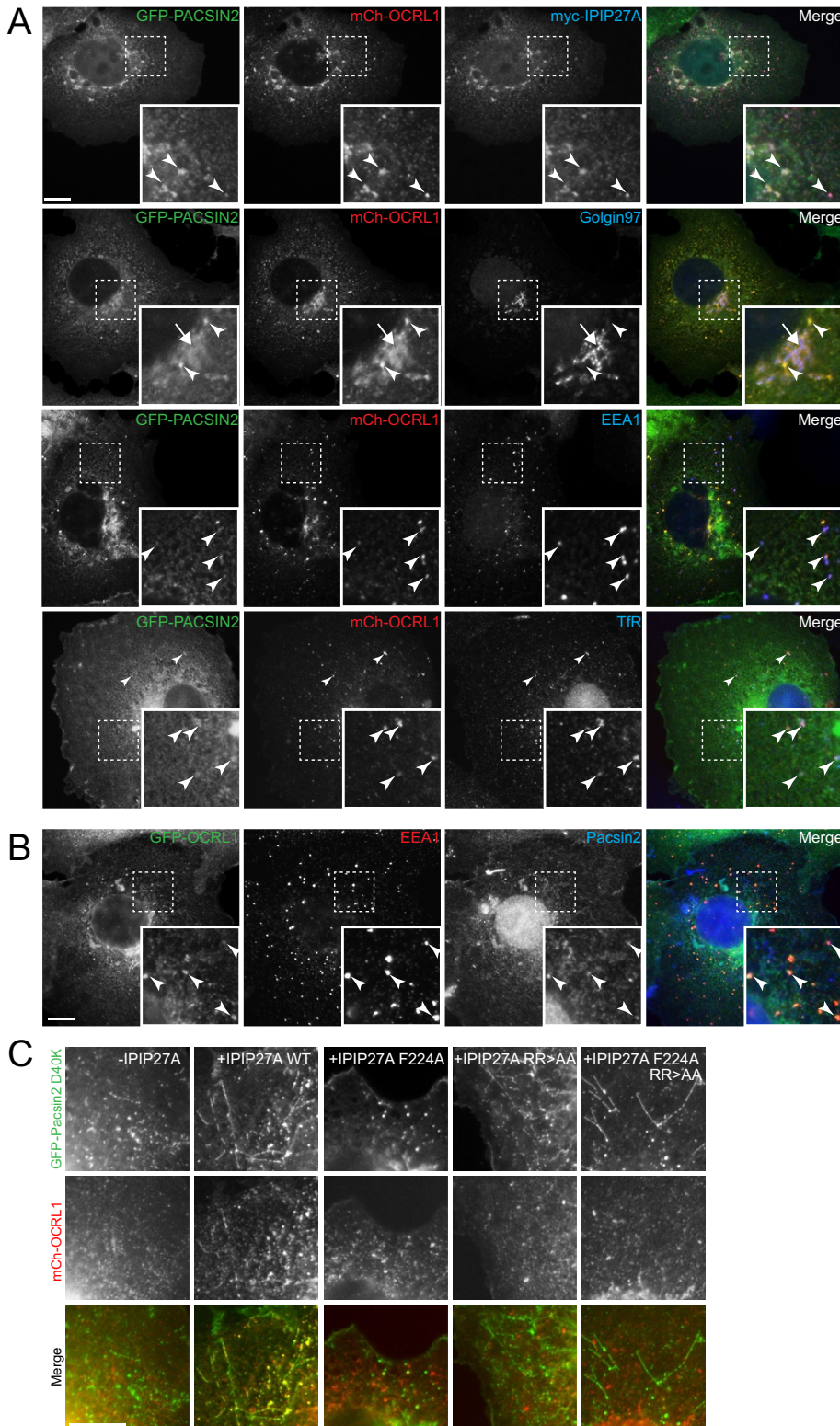
OCRL1 regulates carrier biogenesis |

FIGURE 2: Pacsin 2 localization to endosomes and the Golgi apparatus. (A) COS-7 cells transiently transfected with GFP-pacsin 2, mCherry-OCRL1, and myc-IPIP27A were fixed, immunolabeled with antibodies raised against the myc epitope, golgin97, EEA1, or TfR (blue), as indicated, and examined by immunofluorescence microscopy. (B) COS-7 cells transiently transfected with GFP-OCRL1 were fixed, immunolabeled with antibodies raised against EEA1 (red) and pacsin 2 (blue) as indicated, and examined by immunofluorescence microscopy. Arrowheads indicate colocalization on endosomes, and the arrow denotes colocalization on the TGN. (C) COS-7 cells transiently transfected with GFP-pacsin 2 D40K and mCh-OCRL1 with or without coexpression of the indicated myc-tagged IPIP27A construct were examined by fluorescence microscopy. Scale bars, 10 μm.

acts in a dominant-negative manner to perturb endocytic traffic (Hyvola et al., 2006; Hou et al., 2011). Strikingly, the coexpression of GFP-OCRL1ΔPIP2 together with IPIP27A resulted in elongated tubules emanating from the perinuclear region and peripheral endosomal compartments that contained both proteins (Figure 5A). GFP-CIMPR was present in the tubules, mainly in discrete foci found along the tubule length (Figure 5B). The tubules were not observed when wild-type OCRL1 was coexpressed with IPIP27A, when OCRL1ΔPIP2 was expressed in the absence of IPIP27A, or in the presence of IPIP27B, which cannot bind pacsin 2 (Figure 5A). These observations suggest that OCRL1ΔPIP2 must engage with IPIP27A, and in turn pacsin 2, to cause membrane tubulation. This was confirmed by expressing mutant IPIP27A, unable to bind OCRL1 (F224A) or pacsin 2 (RRAA), both of which failed to support OCRL1ΔPIP2-dependent membrane tubulation (Figure 5D). Taken together, these results support a functional role for the pacsin 2-IPIP27A-OCRL1 complex in regulating TGN and endosomal membrane dynamics.

CIMPR tubulation depends on both F-actin and microtubules

Previous studies indicated a role for OCRL1 in regulating actin dynamics at various cellular locations, where its ability to dephosphorylate PtdIns(4,5)P_2 promotes localized actin turnover (Suchy and Nussbaum, 2002; Dambournet et al., 2011; Bohdanowicz et al., 2012; Kuhbacher et al., 2012; Marion et al., 2012; van Rahden et al., 2012; Nandez et al., 2014). Given that actin plays an important role in carrier biogenesis at the TGN and endosomes (Anitei and Hoflack, 2011), and the fact that pacsin 2 is intimately associated with the actin cytoskeleton (Kessels and Qualmann, 2004; Kostan et al., 2014; Quan and Robinson, 2014), we reasoned that OCRL1, through binding via IPIP27A to pacsin 2, may function to locally regulate actin turnover during carrier morphogenesis and/or promote removal of actin after carrier scission. In support of this hypothesis, we observed excessive accumulation of actin in the perinuclear region and on endosomes upon IPIP27A depletion (Figure 6A). This is similar to what was previously reported for OCRL1 deficiency (Vicinanza et al., 2011). Next we investigated whether the formation of aberrant CIMPR carriers in IPIP27A-depleted cells was dependent upon actin. To probe actin involvement, we treated cells with the actin polymerization inhibitor latrunculin A and monitored CIMPR dynamics. In control
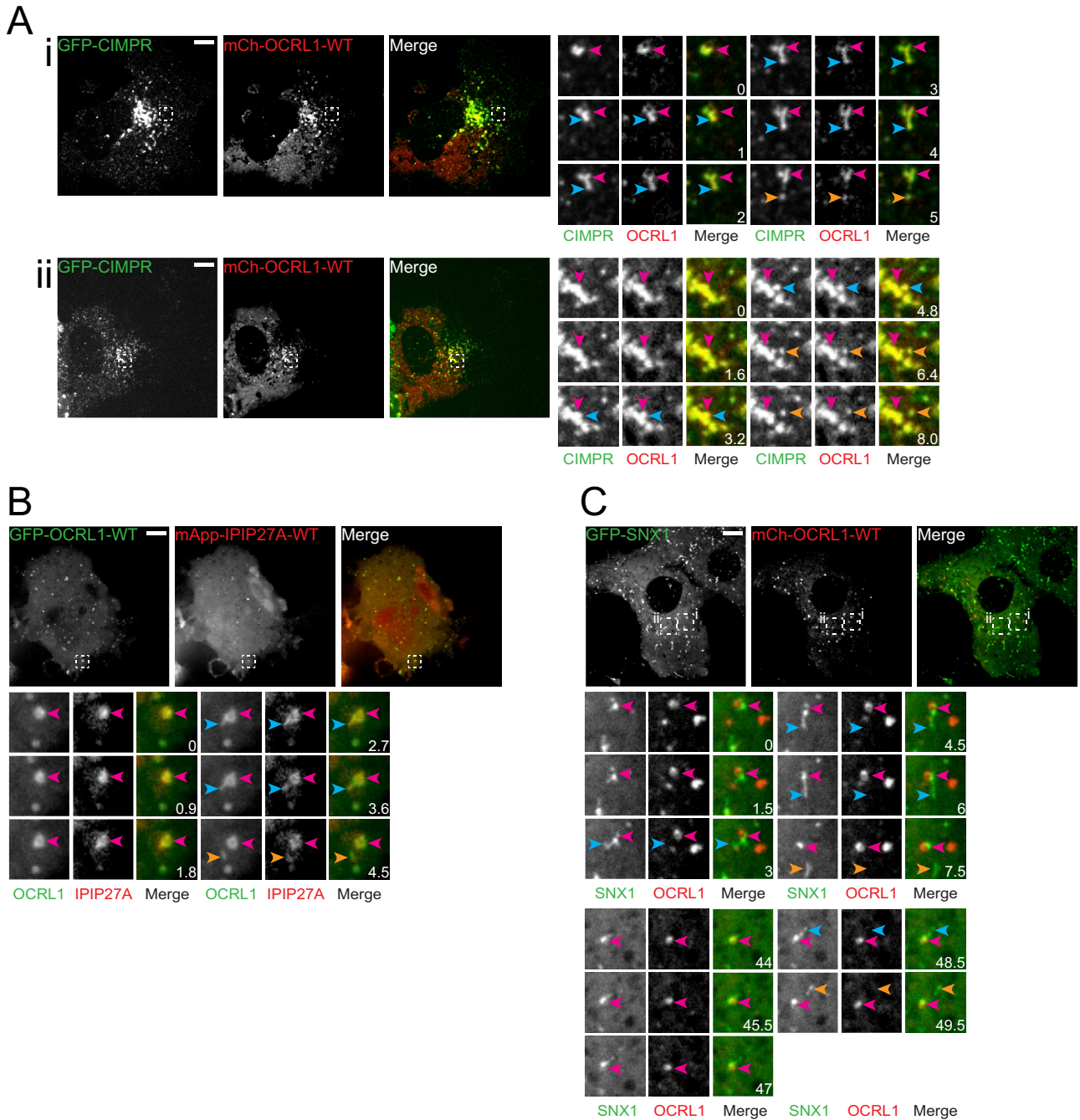
FIGURE 3: OCRL1 and IPIP27A are present on endosome- and TGN-derived trafficking intermediates. (A) COS-7 cells were transfected with GFP-CIMPR, mCh-OCRL1, and myc-IPIP27A and imaged live at 37°C 24 h posttransfection using spinning-disk confocal microscopy. (i, ii) Two different cells indicating budding from an endosome (i) or from the TGN (ii). (B) COS-7 cells were cotransfected with GFP-OCRL1-WT and mApple-IPIP27A and imaged 24 h posttransfection at 37°C using spinning-disk confocal microscopy. (C) COS-7 cells were cotransfected with GFP-SNX1, mCh-OCRL1, and myc-IPIP27A and imaged 24 h posttransfection at 37°C using spinning-disk confocal microscopy. For each experiment, budding events are shown, with the time elapsed in seconds. In all cases, the pink arrowheads indicate the parent structure, the blue arrowheads show where the carrier is emerging, and the orange arrowheads indicate when the carrier has detached from the parent structure. Scale bars, 10 μm.

cells, latrunculin A treatment reduced the formation of CIMPR tubules (Figure 6B), in line with previous studies showing that actin is required for CIMPR carrier biogenesis (Waguri *et al.*, 2003; Anitei *et al.*, 2010). Strikingly, latrunculin A treatment abrogated formation of CIMPR tubules in IPIP27A-depleted cells, confirming that they are also actin dependent (Figure 6B). To further probe actin

involvement, we depleted the actin nucleation–promoting factors (NPFs) neural Wiskott–Aldrich syndrome protein (N-WASP) and the WASH complex. N-WASP functions in carrier biogenesis at the TGN (Anitei and Hoflack, 2011) and has also been implicated in regulating an OCRL1-sensitive pool of endosomal actin (Vicinanza *et al.*, 2011). Of interest, N-WASP binds to and is activated by
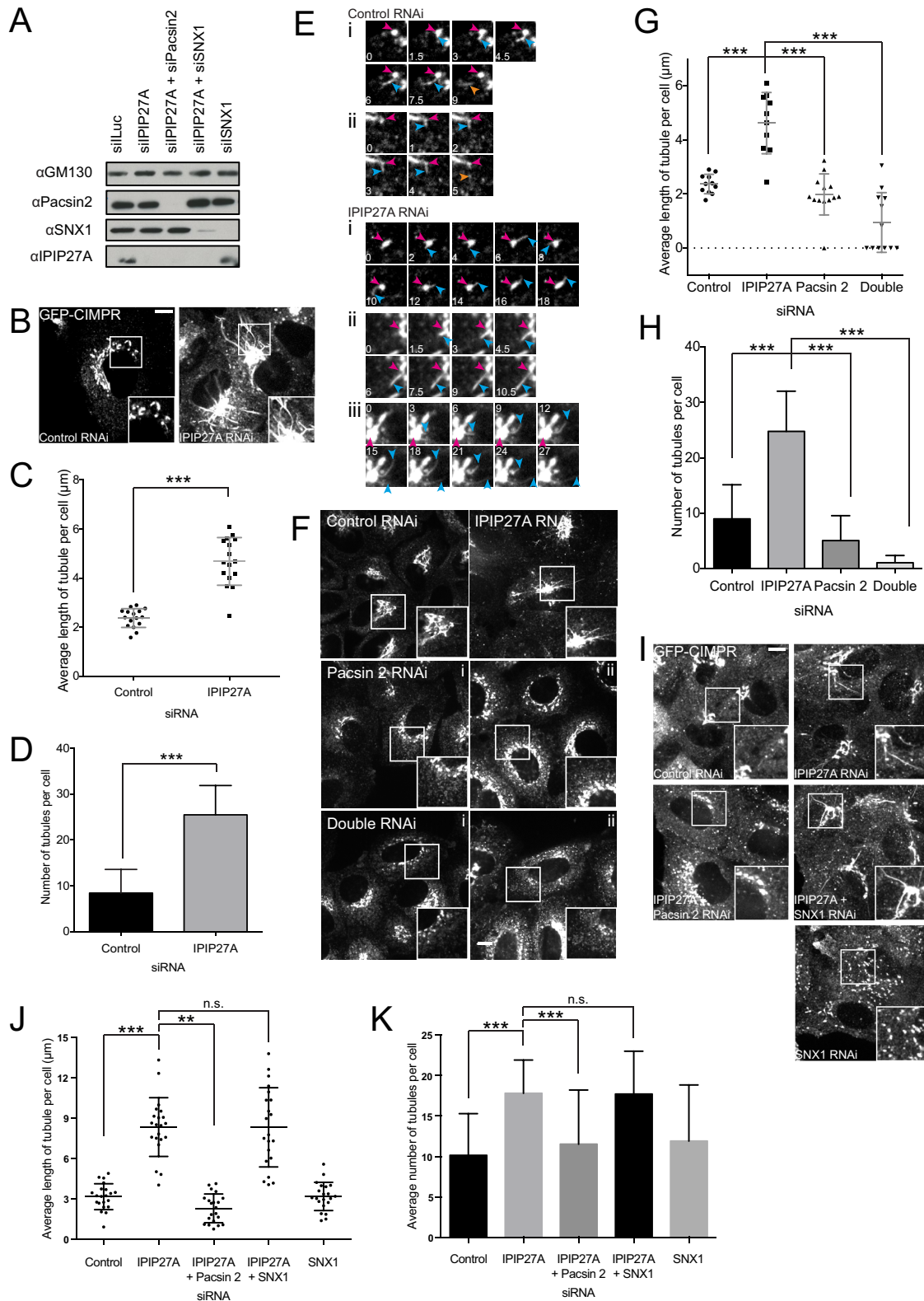
FIGURE 4: Effects of IPIP27A and pacsin depletion upon CIMPR dynamics. (A) HeLaM cells stably expressing GFP-CIMPR were subjected to RNAi as indicated and Western blotting performed 72 h posttransfection with the indicated antibodies. (B–E) HeLaM cells stably expressing GFP-CIMPR were subjected to RNAi as indicated and imaged 72 h posttransfection at 37°C using spinning-disk confocal microscopy. Insets in B show magnifications of the boxed regions. (C) The length of GFP-CIMPR tubules from 16 control (luciferase) or IPIP27A-depleted cells from three independent experiments was measured, and the average tubule length in each cell was calculated. The overall mean tubule length for each condition is also indicated, with the SD shown by the error bars. Means of control and IPIP27A-depleted cells were compared using an unpaired t test using Welch's correction; ***$p < 0.001$. (D) The mean number of GFP-CIMPR

PtdIns(4,5)P$_2$ (Miki *et al.*, 1996) and can bind directly to pacsin 2 (Kessels and Qualmann, 2004). The WASH complex is a major regulator of endosomal actin assembly and is important for several recycling pathways (Derivery *et al.*, 2009; Gomez and Billadeau, 2009; Duleh and Welch, 2010). Of interest, depletion of either N-WASP or WASH strongly impaired the formation of CIMPR tubules seen upon IPIP27A depletion (Figure 6C).

Previous work showed that CIMPR carrier biogenesis depends on microtubules in addition to actin (Waguri *et al.*, 2003). We therefore investigated whether the aberrant CIMPR tubules seen in IPIP27A-depleted cells required intact microtubules. The tubules aligned with microtubules (Figure 6D), and microtubule depolymerization induced by the drug nocodazole led to a complete abrogation of membrane tubulation (Figure 6E). Taken together, our results indicate that both F-actin and microtubules are required for the generation of tubular TGN and endosome-derived CIMPR carriers in IPIP27A-depleted cells.

OCRL1 5-phosphatase activity regulates CIMPR carrier biogenesis

To investigate the requirement for OCRL1 in CIMPR carrier biogenesis, we stably expressed GFP-CIMPR at low levels in control and OCRL1-deficient Lowe syndrome fibroblasts (Figure 7A). In control cells, GFP-CIMPR was localized to the perinuclear TGN and more peripheral endosomes, as expected (Figure 7B). Time-lapse imaging revealed formation of vesicular and short tubular CIMPR carriers at both compartments (Figure 7B). In Lowe syndrome fibroblasts, the steady-state distribution of GFP-CIMPR was similar to that in control cells (Figure 7B). However, time-lapse analysis revealed that CIMPR was more tubular in the Lowe syndrome cells, corresponding to aberrant formation of trafficking intermediates at the TGN and endosomes (Figure 7B). The phenotype was less dramatic than that seen upon IPIP27A depletion, possibly due to redundancy of OCRL1 with the related phosphatase INPP5B, which also binds to IPIP27A (Swan *et al.*, 2010; Noakes *et al.*, 2011). Quantitation revealed that the number of tubules was significantly increased in the Lowe syndrome cells, although tubule length was unaltered (Figure 7, C and D). To determine whether the 5-phosphatase activity of OCRL1 is important for CIMPR carrier formation, we performed rescue experiments. Expression of low levels of wild-type OCRL1 rescued the tubulation phenotype, restoring the number of tubules to control levels (Figure 7, E and F). In contrast, expression of catalytically inactive

OCRL1 (D422A) failed to rescue tubulation, indicating the importance of 5-phosphatase activity for OCRL1 function in CIMPR carrier biogenesis. Moreover, mutant OCRL1 deficient in binding to the F&H motif of IPIP27 (W739A; Pirruccello *et al.*, 2011) was also unable to rescue tubulation, further indicating the importance of the OCRL1-IPIP27A interaction in regulating CIMPR dynamics.

OCRL1 5-phosphatase activity is curvature sensitive and stimulated by tripartite complex formation with IPIP27A and pacsin 2

The IPIP27A-mediated linking of OCRL1 to pacsin 2 would be predicted to enrich OCRL1 in domains of high membrane curvature such as those found at the neck of budding vesicles or tubules. Hence formation of the tripartite OCRL1/IPIP27A/pacsin 2 complex may represent a mechanism for enriching OCRL1 5-phosphatase activity to trafficking intermediates at a late stage in their biogenesis. Previous work showed that the activity of another 5-phosphatase, synaptojanin, is sensitive to membrane curvature (Chang-Ileto *et al.*, 2011). We therefore examined whether the same was true for OCRL1. For this purpose, we incubated recombinant OCRL1 with liposomes of different curvature. As shown in Figure 8A, OCRL1 5-phosphatase activity is higher toward PtdIns(4,5)P$_2$ in high-curvature liposomes (30 nm) than in those with lower curvature (200 nm). The degree of stimulation is comparable to that seen with synaptojanin (Chang-Ileto *et al.*, 2011). Next we assessed whether binding of IPIP27A in the absence or presence of pacsin 2 would affect OCRL1 5-phosphatase activity (performed using 200-nm liposomes). IPIP27A alone resulted in a small (25–50%) but consistently observed reduction in OCRL1 5-phosphatase activity (Figure 8B). However, when the reaction was supplemented with pacsin 2, allowing tripartite complex formation, there was a dramatic stimulation of OCRL1 5-phosphatase activity (sevenfold increase, achieved at a 1:1 M ratio of IPIP27A to pacsin 2; Figure 8B). The interactions between OCRL1, IPIP27A, and pacsin 2 are required for stimulation. Mutant versions of IPIP27A deficient in binding to OCRL1 (F224A) or pacsin 2 (RR>AA) or a pacsin 2 mutant deficient in IPIP27A binding (P428L) failed to stimulate activity (Figure 8C). Note also the loss of inhibition of OCRL1 activity with the F224A mutant of IPIP27A, confirming that the interaction between OCRL1 and IPIP27A is required for this inhibitory effect (Figure 8C). In contrast, abrogation of the IPIP27A–pacsin interaction does not affect the IPIP27A-mediated inhibition of OCRL1 activity (Figure 8C).

tubules per cell for each condition is indicated, with the SD of the samples shown by error bars. Means of control vs. IPIP27A-depleted cells were compared using a Mann–Whitney test; ***$p < 0.001$. (E) Time series of the indicated RNAi-treated cells, showing examples of carrier formation. The pink arrowheads indicate the parent structure, with the blue arrowheads highlighting an emerging carrier or tubule. The orange arrowheads indicate detachment of carriers in control-depleted cells. Times are indicated in seconds. (F–H) Cells were treated with luciferase (control), IPIP27A, or pacsin 2 siRNA independently or with IPIP27A and pacsin 2 siRNA used together (Double) and imaged 72 h posttransfection at 37°C using spinning-disk confocal microscopy. Insets indicate the zoomed areas. (G) The lengths of GFP-CIMPR tubules in the depleted cells (10–13 cells/condition from two independent experiments) were measured, and the average tubule length per cell is plotted on the graph as individual data points. The error bars indicate the SD. Medians were compared using a Kruskal–Wallis test, and adjusted p values calculated using Dunn's multiple comparison test are shown; *$p < 0.05$, **$p < 0.01$, ***$p < 0.001$. (H) The average number of GFP-CIMPR tubules per cell for each condition. Error bars show the SD. Means were compared using one-way ANOVA, and adjusted p values were calculated using a Dunnett multiple comparison test; ***$p < 0.001$. (I–K) Cells were treated with the indicated siRNA and imaged 72 h posttransfection at 37°C using spinning-disk confocal microscopy. Insets indicate the zoomed areas. (J) The lengths of GFP-CIMPR tubules in the depleted cells (21 cells/condition from three independent experiments) were measured, and the average tubule length per cell is plotted on the graph as individual data points. The error bars indicate the SD. (K) Average number of GFP-CIMPR tubules per cell for each condition. Error bars show the SD. Means were compared using one-way ANOVA, and adjusted p values were calculated using a Dunnett multiple comparison test; **$p < 0.01$, ***$p < 0.001$. Scale bars, 10 μm.
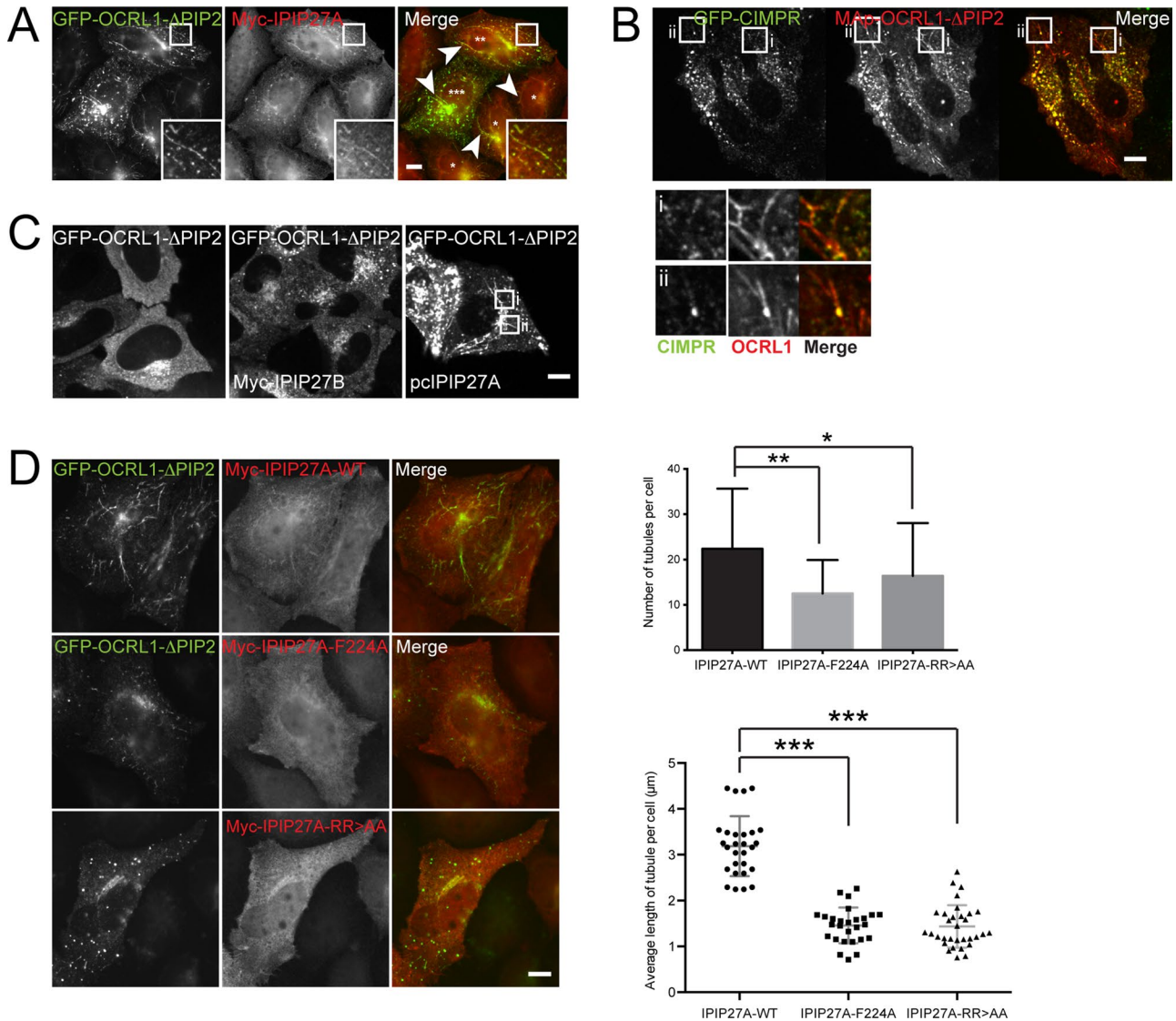
FIGURE 5: Overexpression of OCRL1ΔPIP2 in the presence of IPIP27A causes membrane tubulation. (A) HeLaM cells coexpressing GFP-OCRL1ΔPIP2 (green) and Myc-IPIP27A were labeled with anti-Myc antibody (red) and imaged by fluorescence microscopy. Arrowheads indicate tubules present in the periphery and perinuclear regions of the cell. Asterisks indicate cells with low (*), medium (**) and high (***) GFP-OCRL1ΔPIP2 expression. (B) HeLaM cells stably expressing GFP-CIMPR (green) were transfected with mApple-OCRL1ΔPIP2 (red) and untagged IPIP27 and imaged at 37°C using spinning-disk confocal microscopy at 24 h posttransfection. (C) HeLaM cells were transfected with GFP-OCRL1ΔPIP2 alone or with GFP-OCRL1ΔPIP2 and either pcIPIP27A or Myc-IPIP27B. The cells were imaged as in B. (D) HeLaM cells were cotransfected with GFP-OCRL1ΔPIP2 (green) and Myc-tagged IPIP27A wild type (WT), the F224A OCRL1-binding mutant, or the RR > AA pacsin 2 binding mutant and fixed 24 h posttransfection. Cells were labeled with anti-Myc antibodies (red) and analyzed by fluorescence microscopy. The number and lengths of tubules in 14–16 cells/transfection in three independent experiments were counted. The top graph shows the average number of tubules per cell; error bars indicate SDs. Means were compared using one-way ANOVA, and adjusted p values calculated using Dunnett's multiple comparison test are shown; *$p = 0.244$, **$p = 0.0001$. For the bottom graph, the lengths of tubules in 14–16 cells/transfection (two independent experiments) were measured and an average tubule length for each cell calculated and plotted. The means are indicated with error bars showing the SD. Means were compared using one-way ANOVA with Dunnett's multiple comparison test; ***$p < 0.001$.

To better understand the mechanism of OCRL1 regulation, we repeated the experiments with a pacsin 2 mutant deficient in generating membrane curvature (K147E/K148E/K150E; Rao et al., 2010). As shown in Figure 8D, this mutant failed to stimulate OCRL1 5-phosphatase activity, confirming the importance of membrane curvature for OCRL1 activation. Of interest, stimulation of OCRL1 activity with wild-type pacsin 2 was also observed

with 30-nm liposomes (Figure 8E). Pacsin 2 can therefore promote OCRL1 activity by generating curvature or promoting association with preexisting high-curvature membranes, both of which depend on the F-BAR domain. We also tested whether SNX9, a BAR domain protein that can bind directly to OCRL1 (Nandez et al., 2014), would affect 5-phosphatase activity. As shown in Figure 8F, OCRL1 5-phosphatase activity was
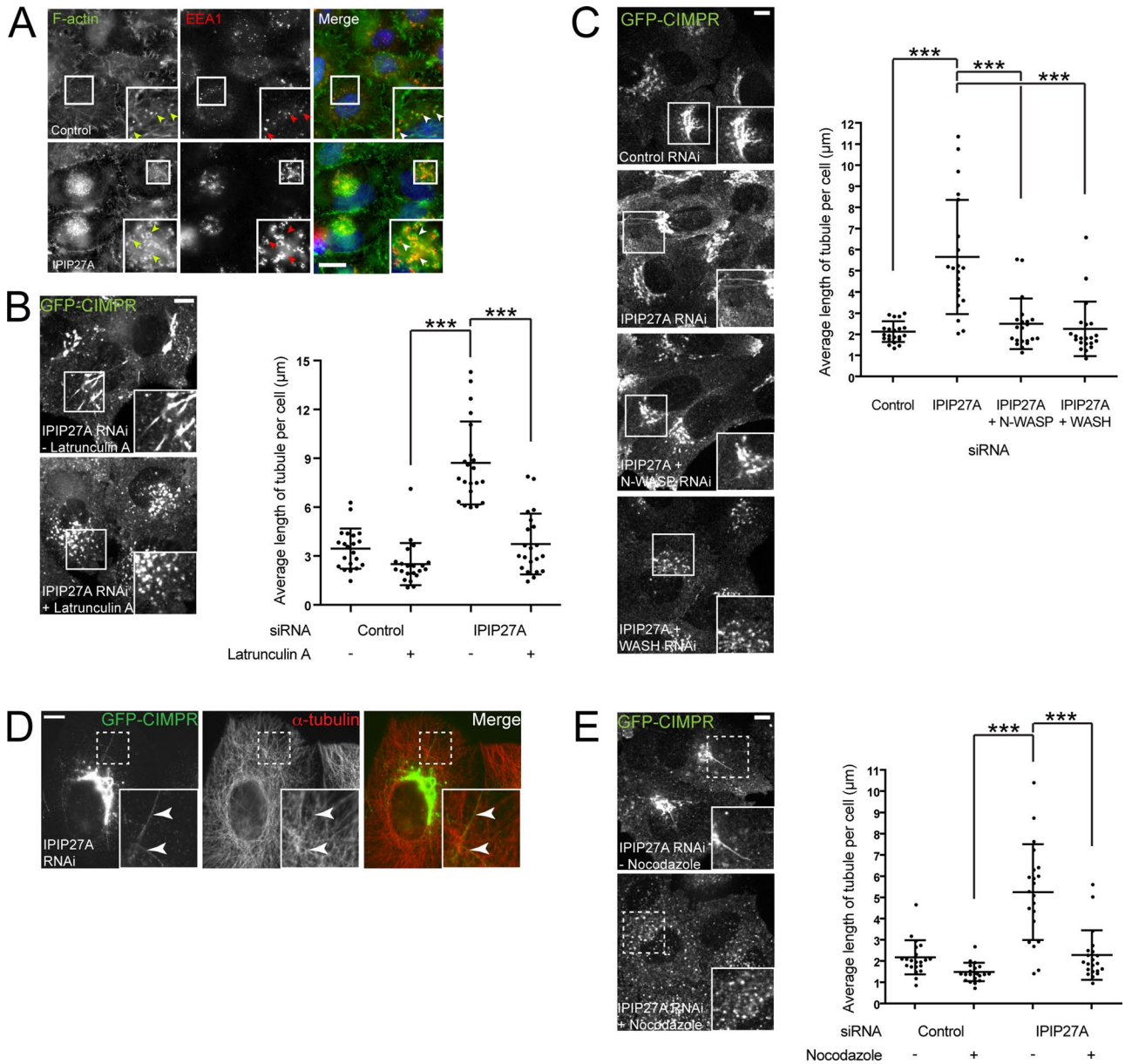
FIGURE 6: CIMPR tubules induced by IPIP27A depletion require the actin cytoskeleton and microtubules. (A) HeLa cells treated with control (luciferase) or IPIP27A siRNA were fixed and labeled for actin using Alexa 488–phalloidin (green), together with an antibody raised against EEA1 (red). (B) HeLaM cells stably expressing GFP-CIMPR were treated with the indicated siRNA, then, at 72 h posttransfection, incubated in the absence or presence of 0.2 μM latrunculin A for 1 h at 37°C, and then imaged using spinning-disk confocal microscopy. Insets indicate the zoomed areas. The length of tubules from 21 cells from three independent experiments was measured for each treatment, and the average tubule length in each cell was calculated. (C) HeLaM cells stably expressing GFP-CIMPR were treated with the indicated siRNA, and imaged 72 h posttransfection at 37°C using spinning-disk confocal microscopy. Insets indicate the zoomed areas. The length of GFP-CIMPR tubules from 21 cells from three independent experiments was measured for each treatment, and the average tubule length in each cell was calculated. (D) HeLaM cells stably expressing GFP-CIMPR were treated with the indicated siRNA and, 72 h later, fixed and immunolabeled with an antibody raised against α-tubulin. (E) HeLaM cells stably expressing GFP-CIMPR were treated with the indicated siRNA, then, 72 h posttransfection, incubated in the absence or presence of 10 μM nocodazole for 2 h at 37°C, and then imaged using spinning-disk confocal microscopy. Insets indicate the zoomed areas. The length of tubules from 21 cells from three independent experiments was measured for each treatment, and the average tubule length in each cell was calculated. For all data, medians were compared using a Kruskal–Wallis test, and adjusted p values calculated using Dunn's multiple comparison test are shown; ***$p < 0.001$. Scale bars, 10 μm.

unaffected by SNX9. Taken together, these results indicate that IPIP27A-mediated linking of OCRL1 to the F-BAR protein pacsin 2 stimulates its 5-phosphatase activity in a membrane curvature–dependent manner.

OCRL1 5-phosphatase activity promotes dissolution of pacsin 2 tubules

Pacsin 2 binds to acidic lipids, including phosphatidic acid, and phosphoinositides such as PtdIns(4,5P)$_2$ (Quan and Robinson, 2014).
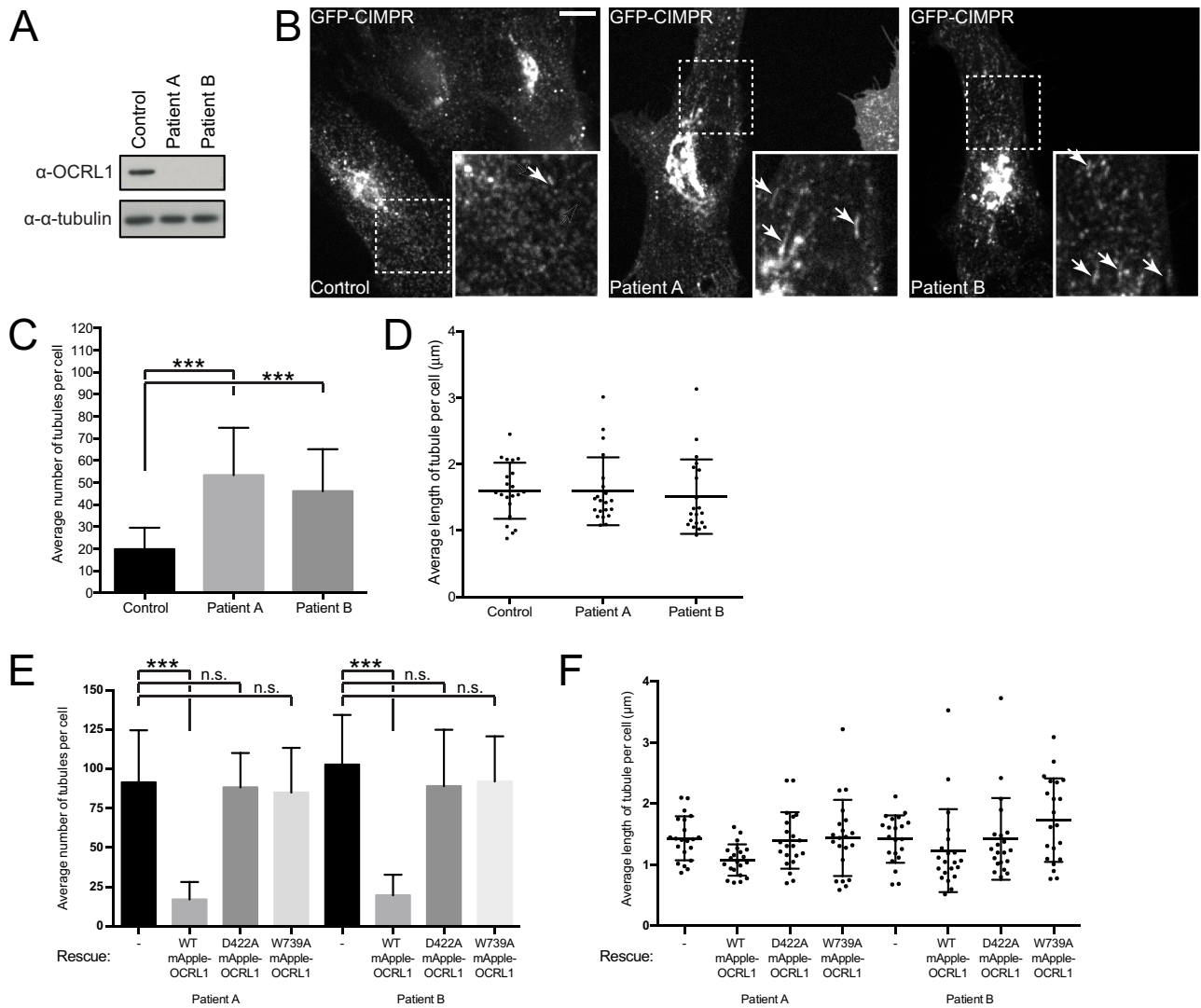
FIGURE 7: CIMPR dynamics in Lowe syndrome patient fibroblasts. Dermal fibroblasts derived from either one of two Lowe syndrome patients (Patient A, Patient B) or from a control patient were lentivirally transduced with GFP-CIMPR. (A) Western blot of cell lysates from GFP-CIMPR–expressing control or patient fibroblasts, using antibodies raised against the indicated antigens. (B–D) GFP-CIMPR–expressing control or patient fibroblasts were imaged at 37°C using spinning-disk confocal microscopy. Insets indicate the zoomed areas, with arrows denoting tubules. Scale bar, 10 µm. (C) Number of tubules from 21 control or patient cells from three independent experiments was measured, and the mean tubule number was calculated, with the SD shown by the error bars. Medians were compared using a Kruskal–Wallis test, and adjusted p values calculated using Dunn's multiple comparison test are shown; ***$p < 0.001$. (D) Average tubule length in each cell was also calculated, with the SD shown by the error bars. (E, F) Lowe syndrome patient cells stably expressing GFP-CIMPR were lentivirally transduced with mApple OCRL1 WT, D422A, or W739A and imaged at 37°C using spinning-disk confocal microscopy. (E) Number of tubules from 21 control or patient cells from three independent experiments was measured, and the mean tubule number was calculated, with the SD shown by the error bars. Means were compared using one-way ANOVA, and adjusted p values calculated using Dunnett's multiple comparison test are shown; ***$p < 0.001$. (F) Average tubule length in each cell was also calculated, with the SD shown by the error bars.

This raised the possibility that OCRL1-mediated PtdIns(4,5P)$_2$ hydrolysis could influence the membrane binding or tubulation properties of pacsin 2. To test this hypothesis, we took advantage of a rapamycin-based heterodimerization assay to inducibly recruit the OCRL1 catalytic domain to ectopically generated pacsin 2 tubules. As shown previously (Rao *et al.*, 2010; Shimada *et al.*, 2010), overexpression of the pacsin 2 F-BAR domain, in this case fused to GFP and the rapamycin-binding domain of mTOR (FRB), induced extensive membrane tubulation when expressed in cells (Figure 8, G and H).

Pacsin 2 tubules were still prevalent when the 5-phosphatase domain of OCRL1 domain, fused to the FK506-binding protein (FKBP), was coexpressed in the absence of rapamycin (Figure 8, G and H). However, on addition of rapamycin to stimulate pacsin 2-OCRL1 heterodimerization, tubulation was completely abolished (Figure 8, G and H). This effect depended on the 5-phosphatase activity of OCRL1, because catalytically inactive OCRL1 had no effect on pacsin 2–induced tubulation, even though it was efficiently recruited to the tubules (Figure 8, G and H). These results

indicate that OCRL1-catalyzed PtdIns(4,5P)$_2$ hydrolysis has the ability to destabilize membrane association of pacsin 2 and/or promote scission of pacsin 2 membrane tubules in vivo.

Depletion of pacsin 2 impairs CIMPR recycling

Loss of either OCRL1 or IPIP27A impairs MPR trafficking at the TGN/endosome interface (Cui et al., 2010; Noakes et al., 2011; Vicinanza et al., 2011; van Rahden et al., 2012). Our results suggest that OCRL1 and IPIP27A act together with pacsin 2 in generating CIMPR-containing trafficking intermediates. We therefore predict that pacsin 2 is required for CIMPR trafficking at the TGN/endosome interface. To functionally test this possibility, we depleted pacsin 2 by RNA interference and analyzed CIMPR trafficking using a well-characterized chimeric CD8-CIMPR reporter (Seaman, 2004). This reporter offers a convenient way to assess directly endosome-to-TGN delivery of the CIMPR. As shown in Figure 9, A–C, depletion of pacsin 2 inhibited trafficking of CD8-CIMPR from endosomes to the TGN. The extent of trafficking inhibition was comparable to that seen upon IPIP27A depletion (Figure 9, A–C). This result indicates a role for pacsin 2 in recycling of CIMPR from endosomes to TGN, which is also affected by loss of OCRL1 or IPIP27A (Noakes et al., 2011; Vicinanza et al., 2011; van Rahden et al., 2012).

DISCUSSION

Previous studies revealed CIMPR trafficking defects upon loss of OCRL1 (Choudhury et al., 2005; Cui et al., 2010; Vicinanza et al., 2011; van Rahden et al., 2012). However, it has been unclear whether these defects reflect a global perturbation of organelle homeostasis, arising from altered phosphoinositide levels, or indicate a more direct role for OCRL1 in the trafficking process (Pirruccello and De Camilli, 2012). Our findings support the latter hypothesis. IPIP27A links OCRL1 directly to a component of the trafficking machinery, pacsin 2, and we observe OCRL1 in newly formed trafficking intermediates exiting from both TGN and early endosomal compartments. The OCRL1- and IPIP27A-positive CIMPR trafficking intermediates are distinct from those containing SNX1 and lack the endocytic recycling cargoes transferrin receptor and Wls. The close association of OCRL1 with CIMPR trafficking machinery that we observe is in good agreement with a report showing that CIMPR and the AP1-associated clathrin adaptor epsinR are major constituents of OCRL1 complexes isolated from cells (Nandez et al., 2014). Moreover, proteomic fractionation profiling indicates that CIMPR is the most highly correlated protein with IPIP27A, strongly supporting the view that IPIP27A is associated with CIMPR trafficking intermediates (Borner et al., 2014). Based on this method, IPIP27A also correlates well with Vti1B, which binds epsinR, as well as pacsin 2, and OCRL1 is highly correlated with AP1 and epsinR, consistent with the biochemistry of OCRL1 complexes (Borner et al., 2014; Nandez et al., 2014).

Although previous studies focused mainly on the role of OCRL1 and IPIP27A in retrograde endosome-to-TGN traffic (Choudhury et al., 2005; Noakes et al., 2011; Vicinanza et al., 2011; van Rahden et al., 2012), our results support a role for OCRL1 and IPIP27A also in anterograde TGN-to-endosome traffic. This is consistent with the presence of OCRL1 in clathrin-coated buds at the TGN (Choudhury et al., 2005) and the high degree of correlation between IPIP27A and lysosomal hydrolases, which are trafficked in the anterograde TGN-to-endosome direction, seen in proteomic fractionation profiling (Borner et al., 2014). The close association of OCRL1 with CIMPR and lysosomal hydrolase trafficking also helps explain why Lowe syndrome patients have elevated hydrolases in their plasma, which is indicative of missorting at the TGN (Ungewickell and Majerus,

1999). OCRL1 and IPIP27A therefore appear to function in biogenesis of both anterograde and retrograde CIMPR trafficking intermediates at the TGN and early endosome, respectively.

Pacsin 2 preferentially binds to high-curvature membranes, such as those found at the neck of budding vesicles (Qualmann et al., 2011). Indeed, pacsin 2 associates with clathrin-coated buds at the plasma membrane only at a very late stage, immediately before scission, coinciding with the formation of a high-curvature vesicle neck (Qualmann et al., 2011; Taylor et al., 2011). Hence IPIP27A-mediated engagement of pacsin 2 would be expected to recruit OCRL1 to newly forming trafficking intermediates at a late stage, immediately preceding or coinciding with scission. It is known that Rab GTPases are required for targeting OCRL1 to the membrane (Hyvola et al., 2006; Hou et al., 2011). We therefore envisage a model in which OCRL1 is first recruited to the membrane by Rab GTPases, and, once bound to the membrane, engages, via IPIP27A, with pacsin 2 in regions of high membrane curvature corresponding to the neck of late-stage budding intermediates. Before pacsin 2 binding, OCRL1 activity is attenuated by IPIP27A. Once OCRL1 associates with pacsin 2, catalytic activity is stimulated, ensuring that the timing of enzymatic activation and hydrolysis of PtdIns(4,5)P$_2$ coincides with scission or release of the newly formed trafficking intermediate. Perturbation of this mechanism would be expected to lead to a membrane scission defect, which is in accordance with the aberrant CIMPR tubulation we see upon loss of OCRL1 or IPIP27A. An analogous mechanism has been proposed for the activation of synaptojanin on endophilin-generated trafficking intermediates at the plasma membrane (Chang-Ileto et al., 2011).

Our results indicate that OCRL1-mediated PtdIns(4,5)P$_2$ hydrolysis is important for CIMPR carrier biogenesis at the TGN and endosomes. This could reflect a direct physiological role for PtdIns(4,5)P$_2$ in carrier formation at these locations, where it may recruit and/or activate components of the trafficking machinery. PtdIns(4,5)P$_2$ has been detected at the TGN and endosomes (Watt et al., 2002; Shi et al., 2012), and the actin machinery, which is often regulated by PtdIns(4,5)P$_2$, is known to promote carrier biogenesis at both compartments (Anitei and Hoflack, 2011). Moreover, PtdIns4P 5-kinases have been localized to the Golgi and endosomes, indicating that PtdIns(4,5)P$_2$ synthesis can occur at these compartments (Godi et al., 1999; Sun et al., 2013). Of interest, N-WASP, which promotes clathrin and AP1 carrier biogenesis at the TGN (Anitei et al., 2010), is activated by binding to PtdIns(4,5)P$_2$ and pacsin 2, which itself is a PtdIns(4,5)P$_2$-binding protein (Miki et al., 1996; Kessels and Qualmann, 2004). Hence OCRL1 may remove PtdIns(4,5)P$_2$ and in turn promote disassembly of actin and actin-associated machinery during late stages of carrier formation at the TGN and endosomes. Indeed, depletion of IPIP27A leads to ectopic actin accumulation at these compartments, and the aberrant carriers generated in IPIP27A-depleted cells are actin dependent. Another possibility is that OCRL1 functions to remove ectopic PtdIns(4,5)P$_2$ from TGN and endosome carriers. PtdIns(4,5)P$_2$ plays a key role in recruiting adaptors and accessory factors to clathrin-coated pits at the plasma membrane (McMahon and Boucrot, 2011). OCRL1 may contribute to fidelity of carrier formation at the TGN and endosomes by preventing inappropriate recruitment of plasma membrane adaptors, many of which have a high propensity to bind to clathrin, at these locations. PtdIns(4,5)P$_2$ hydrolysis by OCRL1 could therefore be viewed as a proofreading step to ensure correct adaptor incorporation into clathrin buds at the TGN and endosomes. In line with this possibility, ectopic endosomal accumulation of PtdIns(4,5)P$_2$ and its effectors has been reported in OCRL1-deficient cells (Ben El Kadhi et al., 2011; Vicinanza et al., 2011). Of interest, the product
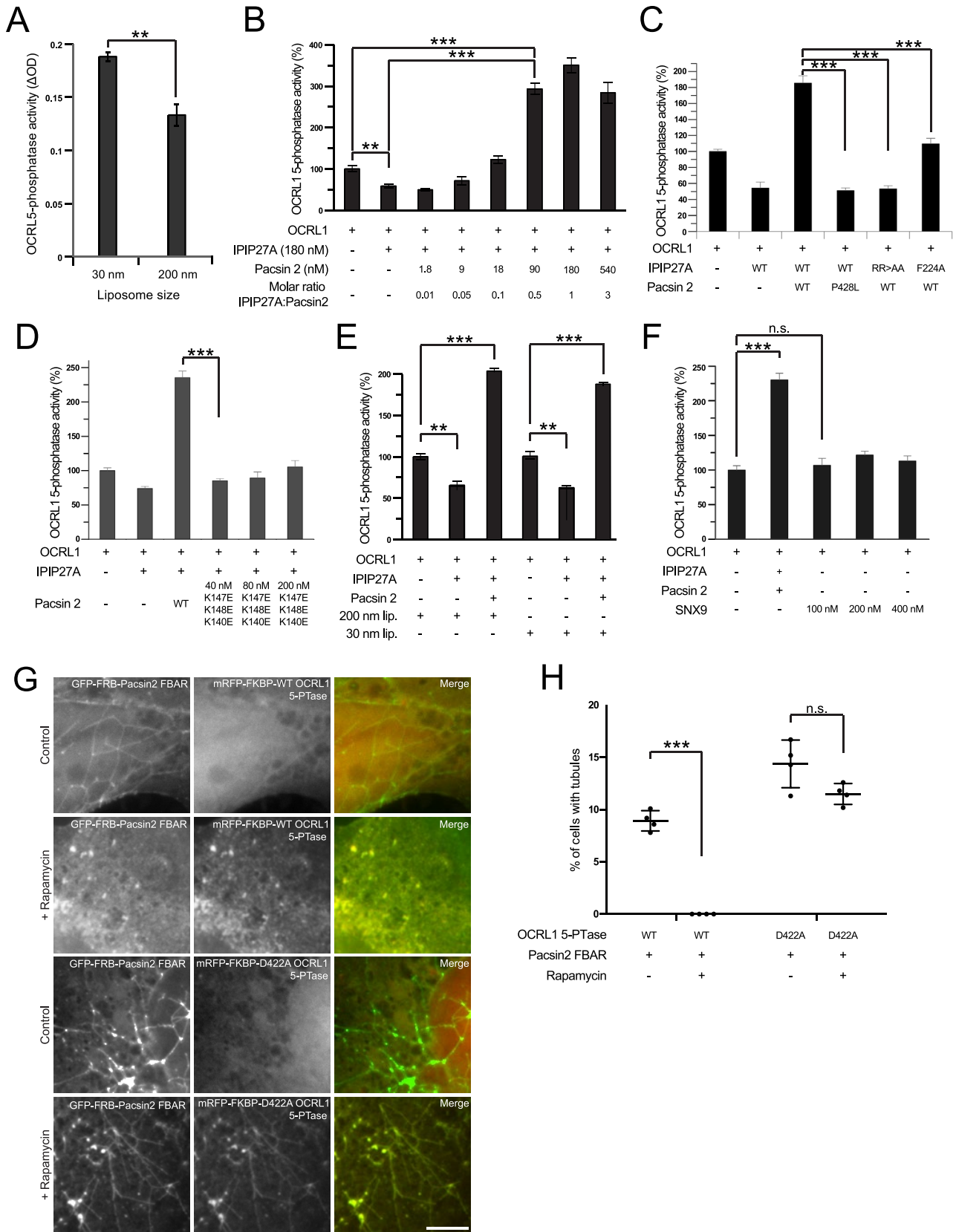
FIGURE 8: OCRL1 5-phosphatase activity is stimulated by tripartite complex formation with IPIP27A and pacsin 2 and by itself promotes dissolution of pacsin 2 tubules. (A–E) OCRL1 5-phosphatase activity was measured using a malachite green assay, as described in *Materials and Methods*, in the presence or absence of the indicated lipid vesicles and proteins. (A) His/S-tagged OCRL1 (30 nM) was incubated with 100 μM of PtdIns(4,5)P2 -containing liposomes of the indicated sizes. (B) His/S-OCRL1 (30 nM) was incubated with 100 μM PtdIns(4,5)P2–containing, 200-nm-diameter
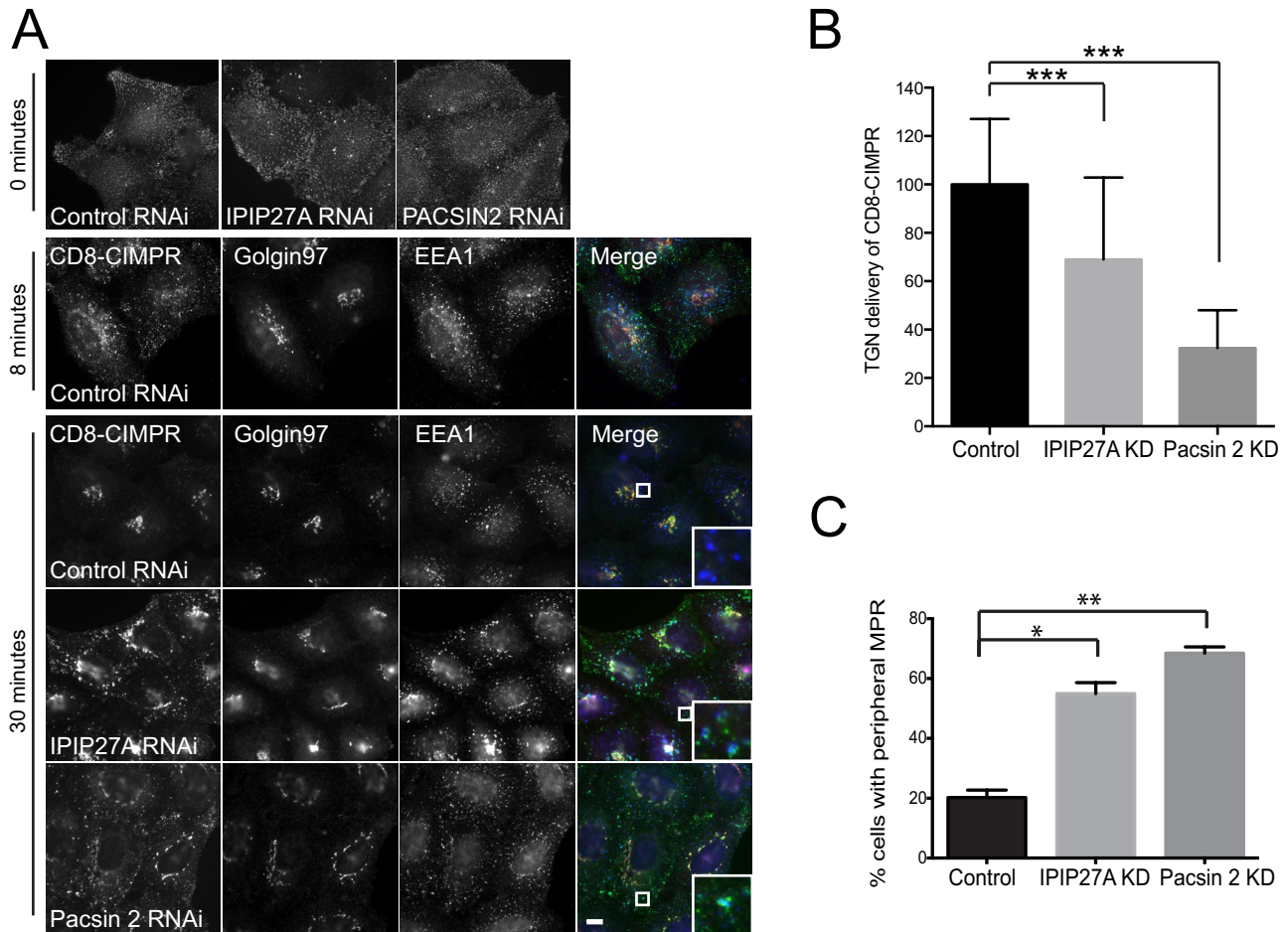
FIGURE 9: Pacsin 2 depletion impairs CIMPR recycling. (A) HeLaM CD8-CIMPR cells treated with luciferase (control), IPIP27A, or pacsin 2 siRNA were incubated on ice with CD8 antibody and either fixed immediately (0 min) or warmed to 37°C for 8 or 30 min before fixation and labeling with antibodies to EEA1 (blue) or golgin97 (red). CD8 was detected with appropriate secondary antibodies (green). Scale bar, 10 μm. (B, C) CD8-CIMPR recycling was quantified by determining the extent of colocalization between endocytosed CD8-CIMPR and golgin97 after incubation at 37°C for 30 min relative to the total CD8-CIMPR fluorescence (B) or the percentage of cells with peripheral (endosomal) CD8 staining at 30 min (C). Results are from two independent experiments ($n = 25$ and 100 cells for each knockdown in B and C, respectively) and are shown as mean + SD. Means were compared using one-way ANOVA, and adjusted p values were calculated using Dunnett's multiple comparison test; ***$p < 0.001$, **$p = 0.003$, *$p = 0.01$.

liposomes in the presence or absence of various concentrations of GST-IPIP27A C-terminal fragment (192–249) and GST-pacsin 2, as indicated. (C) His/S-OCRL1 (30 nM) was incubated with 100 μM PtdIns(4,5)P2–containing, 200-nm-diameter liposomes in the presence or absence of WT or mutant forms of GST-IPIP27A C-terminal fragment (180 nM) or GST-pacsin 2 (36 nM), as indicated. (D) His/S-OCRL1 (30 nM) was incubated with 100 μM PtdIns(4,5)P2–containing, 200-nm-diameter liposomes in the presence or absence of WT IPIP27A C-terminal fragment (180 nM) and either 36 nM WT or the indicated concentrations of a GST-pacsin 2 mutant deficient in membrane tubulation activity, as indicated. (E) His/S-OCRL1 (30 nM) was incubated with 100 μM PtdIns(4,5)P2–containing, 200- or 30-nm-diameter liposomes as indicated in the presence or absence of WT IPIP27A C-terminal fragment (180 nM) and 36 nM GST-pacsin 2. The data set for each liposome size was normalized to 100%. (F) His/S-OCRL1 (30 nM) was incubated with 100 μM PtdIns(4,5)P2–containing, 200-nm-diameter liposomes in the presence or absence of GST-IPIP27A WT C-terminal fragment (180 nM), WT GST-pacsin 2 (36 nM), or various concentrations of GST-SNX9, as indicated. For B–F, data are shown as a percentage of OCRL1 5-phosphatase activity when incubated alone. For A–E, means were compared using either Student's t test (A) or one-way ANOVA (B–F), and adjusted p values calculated using Dunnett's multiple comparison test are shown for the indicated pairwise comparisons; **$p < 0.01$, ***$p < 0.001$. The results are from three independent experiments, each repeated in triplicate. (G, H) COS-7 cells were transiently cotransfected with GFP-FRB-pacsin 2 F-BAR (green) and either the WT or D422A 5-phosphatase domain of OCRL1 fused to mRFP and FKBP (red), as indicated. Cells were then incubated in the presence or absence of 1 μM rapamycin for 1 h at 37°C and then fixed and examined by wide-field microscopy (G). Scale bar, 10 μm. (H) Percentage of cells containing pacsin 2-F-BAR tubules for the indicated conditions in four independent experiments was measured. The error bars show the SD. Means were compared using Student's t test, and p-values are shown; ***$p < 0.001$.

of OCRL1, PtdIns4P, binds to TGN and endosome-associated clathrin adaptors, including epsinR (Santiago-Tirado and Bretscher, 2011). Hence, in addition to removing PtdIns(4,5)P_2, OCRL1 may also act in a positive capacity to promote or stabilize membrane recruitment of PtdIns4P-binding adaptors during clathrin vesicle formation at the TGN and endosomes.

Although our results indicate a role for the OCRL1/IPIP27A/pacsin 2 complex at the TGN and endosomes, we believe the same complex is likely to function in clathrin vesicle biogenesis at the plasma membrane. OCRL1 and pacsin 2 are both present in late-stage clathrin-coated pits (Erdmann et al., 2007; Taylor et al., 2011; Nandez et al., 2014), and proteomic analysis of clathrin-coated vesicle fractions showed that OCRL1 and IPIP27A are present in both plasma membrane– and TGN/endosome-derived vesicles (Hirst et al., 2012). Hence OCRL1 may be similarly regulated by IPIP27A and pacsin 2 during clathrin vesicle biogenesis at the plasma membrane as it is on endomembranes. In contrast, interaction with SNX9, which does not affect OCRL1 catalytic activity, appears restricted to the plasma membrane (Nandez et al., 2014). It is also worth noting that pacsin 2 functions in a number of other processes that require membrane remodeling and actin engagement, including cytokinesis and caveolae formation (Hansen et al., 2011; Senju et al., 2011; Smith and Chircop, 2012; Takeda et al., 2013). It will be interesting to investigate whether OCRL1 participates in these processes through binding via IPIP27A to pacsin 2. Furthermore, because IPIP27A also binds to the related 5-phosphatase INPP5B, it is possible that INPP5B could participate in additional pacsin 2–dependent processes (Swan et al., 2010; Noakes et al., 2011). Further studies are required to examine these possibilities.

MATERIALS AND METHODS

Materials and antibodies
Reagents were obtained from Sigma-Aldrich (St. Louis, MO), Merck (Kenilworth, NJ), or Fisher Scientific (Hampton, NH) unless otherwise specified. The following antibodies were used: sheep anti-IPIP27A and B (Noakes et al., 2011); mouse anti–α-tubulin (Keith Gull, University of Oxford, Oxford, United Kingdom); mouse anti-CD8 (C7423; Sigma-Aldrich); goat anti-EEA1 (N19; Santa Cruz Biotechnology, Dallas, TX); mouse anti-EEA1 (610456; BD Biosciences, Franklin Lakes, NJ); sheep anti-GFP (Diao et al., 2003); sheep anti–glutathione S-transferase (GST; Hyvola et al., 2006); rabbit anti-golgin97 (Nobuhiro Nakamura, Kyoto Sangyo University, Kyoto, Japan); rabbit anti-Myc (C3956; Sigma-Aldrich); mouse anti-SNX1 (611482; BD Biosciences); mouse anti-TfR (H68.4; Zymed, Waltham, MA); and sheep anti-TGN46 (Vas Ponnambalam, University of Leeds, Leeds, United Kingdom). Sheep polyclonal anti–pacsin 2 antibodies were raised against human pacsin 2 by injecting an N-terminal GST-tagged pacsin 2 fragment (amino acids 305–387, corresponding to the region of least similarity to pacsin 1 and 3) into sheep (conducted by the Scottish National Blood Transfusion Service, Edinburgh, United Kingdom). Anti–pacsin 2 antibodies were then purified on glutathione beads (GE Healthcare) using the same antigen. Alexa 594 and 647–conjugated phalloidin were bought from Molecular Probes. Alexa 488– and 594–conjugated and Cy3- and Cy5-conjugated secondary antibodies were from Molecular Probes (Eugene, OR) and Jackson ImmunoLabs (West Grove, PA), respectively. Horseradish peroxidase–conjugated secondary antibodies were from Santa Cruz Biotechnology or Tago Immunochemicals (Limerick, PA).

Molecular biology
IPIP27A and OCRL1 (isoform a) constructs have been described previously (Choudhury et al., 2005; 2009; Noakes et al., 2011). Additional point mutants were generated by PCR using the QuikChange method (Stratagene, La Jolla, CA). Standard molecular biology methods were used to clone pacsin 2 (IMAGE clone 5173129) into pEGFP-C2 (BD Biosciences) or a modified pcDNA3.1(-) (Stratagene) containing an N-terminal mCherry tag, and point mutations were introduced as described to generate the P478L and D40K mutants for expression in mammalian cell lines. Tagged OCRL1 and IPIP27A were cloned into the XLG3 vector (kindly provided by Peter Cullen, University of Bristol, Bristol, United Kingdom) by standard molecular biology methods. Similarly, GFP-CIMPR (cDNA kindly provided by Matthew Seaman, University of Cambridge, Cambridge, United Kingdom) was also cloned into the XLG3 vector. For bacterial expression of recombinant pacsin 2 proteins for antibody production, a fragment encompassing amino acids 305–387 was cloned into pGex-4T-2. Similarly, for bacterial expression of recombinant GST-tagged pacsin 2 and SNX9 used in lipid phosphatase assays, DNA encoding full-length protein was cloned into pGEX-4T-2. For the rapamycin-based heterodimerization assay, the F-BAR domain of pacsin 2 was inserted 3′ to GFP and the rapamycin-binding domain of mTOR (FRB) to generate GFP-FRB-pacsin 2 F-BAR. The 5-phosphatase domain of OCRL1 (amino acids 237–539) was inserted 3′ to monomeric red fluorescent protein (mRFP) and FKBP to generate mRFP-FKBP-OCRL1 5-PTase, with site-directed mutagenesis used to create a D422A mutant deficient in 5-phosphatase activity. All constructs were verified by sequencing using GATC Biotech (Konstanz, Germany). Primers were synthesized by MWG Biotech (Ebersburg, Germany), and sequences for all manipulations are available upon request. The GFP-TfR and GFP-Rab constructs were a kind gift from Philip Woodman (University of Manchester, Manchester, United Kingdom). The GFP-SNX1 construct was a kind gift of Peter Cullen (University of Bristol), and the GFP-Wls construct was a kind gift of Barth Grant (Rutgers University, New Brunswick, NJ).

Cell culture, transfection, and RNA interference
HeLa, HeLaM, and COS-7 cells were cultured at 37°C and 5% CO_2 in DMEM supplemented with 10% Hyclone fetal bovine serum (Thermo Scientific, Waltham, MA), 1% penicillin/streptomycin (100 U/ml), and 1 mM L-glutamine. Human dermal fibroblasts (ATCC) and Lowe syndrome patient fibroblasts (Baylor College of Medicine, Houston, TX) were grown in the same DMEM-based medium, with the addition of 1% nonessential amino acid solution (Sigma-Aldrich). HelaM cells stably expressing CD8-CIMPR or GFP-CIMPR (kindly provided by Matthew Seaman, University of Cambridge) were grown in the same medium supplemented with 0.5 mg/ml G418. Immortalized human retinal pigment cells (hTERT RPE-1) were cultured in DMEM/F12 supplemented as described (minus G418) and with the addition of 10 µg/ml hygromycin B. Cells were cultured in antibiotic-free medium for all RNAi experiments. DNA transfections were performed with X-tremeGENE HP or FuGENE HD (Roche Diagnostics, Risch-Rotkrequz, Switzerland) according to the manufacturer's instructions. A total of 1 µg DNA per 3.5-cm dish was used. Cells were assayed between 18 and 24 h after transfection. RNAi was performed using Interferin (Polyplus, Illkirch-Graffenstaden, France) and 20 nM siRNA. Cells were assayed 72 h after transfection. For IPIP27A and pacsin 2 KD, the following oligos were used: IPIP27A (1, GUGCUGACCUAGUGGCGGA; 4, GGUGACAGACUCAGCCCAA) and pacsin 2 (2, CCCUUAAUGU-CCCGAGCAA; 4, CUGAGGUGGUUCCGAGCCA). Both oligos for each target displayed the same phenotype. WASH was depleted using the oligos 2, UGUCGGAUCUCUUCAACAA, and 3, GC-CAAGAUUGAGAAGAUCA. N-WASP was depleted with a SMART-pool consisting of four oligos. SNX1 was depleted using the oligo

104 | P. G. Billcliff, C. J. Noakes, Z. B. Mehta, et al.

Molecular Biology of the Cell

AAGAACAAGACCAAGAGCCAC (Carlton et al., 2004). All oligos were obtained from Dharmacon (Lafayette, CO). Luciferase (GL2, CGUACGCGGAAUACUUCGATT; Eurogentec, Liege, Belgium) was used as a negative control.

Lentivirus production

HEK-293LTV cells (Cell Biolabs, San Diego, CA) were cultured to 70–80% confluency in 10-cm dishes. We added 27 µl of branched polyethylenimine (PEI; 1 mg/ml) to 223 µl of serum-free DMEM and incubated at room temperature for 2 min. A 6-µg amount of XLG3 containing mApple-tagged OCRL1 or GFP-CIMPR was diluted with 4.5 µg of psPAX2 and 3 µg of pMD2.G lentiviral packaging vectors (kindly provided by Martin Humphries, University of Manchester) in 250 µl of serum-free DMEM and then mixed with the PEI solution. The cell medium was replaced with 5 ml of prewarmed antibiotic-free medium, and after 20 min of incubation at room temperature, the transfection mixture was added to the cells. After 6–8 h of incubation at 37°C, the medium was replaced with 10 ml of prewarmed antibiotic-free medium and kept at 37°C overnight. The next day, 100 µl of sodium butyrate (1 M stock) was added to the cell medium. The cells were incubated for 8 h at 37°C, and then the medium was replaced with antibiotic-free medium. Medium containing virus was harvested at 72 h, clarified by centrifugation and filtration through a 0.45-µm filter, and stored at −80°C. To infect fibroblast cells, lentivirus solution was added to trypsinized cells at the time of plating (2 ml of virus per 35-cm culture dish). The cells were grown for 72 h, assessed for transduction by fluorescence microscopy, and passaged two or three times before use in experiments.

Generation of IPIP27A-knockout cells by clustered regularly interspaced short palindromic repeats

The guide sequence in the coding region of IPIP27A (GAAGCCTG CATTGTCCAC) was designed and cloned into the pD1301 vector by Horizon Discovery (Waterbeach, UK) and provided as a part of the Horizon clustered regularly interspaced short palindromic repeat reagents for the Knockout Generation Program. HeLaM cells were transfected with the pD1301 plasmid, and 24 h later, the cells were counted and diluted into one 15-cm dish at a density of 300 cells. The dish was grown for 10 d until visible colonies had formed. Individual colonies were trypsinized, reseeded onto 96-well plate wells, and allowed to reach confluency. Fifteen clones were screened for IPIP27A knockout by Western blotting with an anti-IPIP27A antibody, and positive clones were retained and cultured.

CD8-CIMPR trafficking assay

CD8-CIMPR trafficking assays were performed according to Noakes et al. (2011).

Fluorescence microscopy

Cells were grown on coverslips and fixed in either ice-cold methanol for 4 min at −20°C (for staining with anti–α-tubulin) or in paraformaldehyde (PFA; 3% [wt/vol] in phosphate-buffered saline [PBS]) for 20 min at room temperature and then washed three times in PBS. Cells fixed in PFA were permeabilized by incubation in 0.1% Triton X-100 in PBS for 4 min and then washed three times in PBS. Coverslips were incubated for 20 min at room temperature with primary antibodies and then fluorophore-conjugated secondary antibodies (diluted into PBS containing 0.5 mg/ml bovine serum albumin [BSA]) and 100 ng/ml Hoechst 33342 before mounting in Mowiol. Slides were viewed using an Olympus BX60 upright microscope using a 60× objective, and images were taken using a MicroMax cooled, slow scan CCD camera (Roper Scientific, Trenton, NJ) controlled by Metavue software (MDS Analytical Technologies, Sunnyvale, CA). Images were processed using ImageJ (National Institutes of Health, Bethesda, MD) and Adobe Photoshop Creative Suite 5. Figures were assembled in Adobe Illustrator Creative Suite 5. For spinning-disk confocal microscopy cells, were plated in 35-mm glass-bottomed cell culture dishes (MatTek, Ashland, MA) and transfected as described. Cells were imaged using 100% laser power in CO_2-independent medium at 37°C using a Zeiss Axio-Observer Z1 spinning-disk confocal microscope (63× oil objective) with a laser-based Definite Focus system. Movies were captured with a Photometrics Evolve electron-multiplying charge-coupled device camera, and SlideBook software (3i, Denver, CO) was used for image acquisition. Movies were recorded using a range of exposure times as indicated in the legends to the supplemental videos. Times were calculated using 1/acquisition frequency (hertz) to give the total exposure time per frame.

Immunoprecipitation

Cells were lysed on ice for 20 min in HMNT buffer (20 mM 4-(2-hydroxyethyl)-1-piperazineethanesulfonic acid [HEPES], pH 7.4, 5 mM $MgCl_2$, 0.1 M NaCl, 0.5% [wt/vol] Triton X-100, and Protease Inhibitor Cocktail III [Calbiochem, Kenilworth, NJ]) using 500 µl per 10-cm dish. Lysates were clarified by centrifugation at full speed in a microfuge for 10 min at 4°C, followed by the addition of 2 µg of the appropriate primary antibody (per 300 µl of lysate) and incubation at 4°C for 2 h. Immune complexes were collected on 10 µl of protein A or protein G–Sepharose (Invitrogen, Carlsbad, CA) for 1 h at 4°C and analyzed by SDS–PAGE and Western blotting.

Protein-binding experiments

GST-tagged bait protein (10–80 µg) coupled to 10 µl of glutathione-Sepharose was incubated with 250 µl of HNMT cell lysate for 2 h at 4°C. Competition binding with recombinant proteins was performed by coupling 1 µg of GST-IPIP27A C-terminal fragment (amino acids 192–249) to glutathione-Sepharose and incubation in 100 µl of HNMT containing 100 µg/ml of BSA with 3 µg of histidine (His)/S-tagged OCRL1 and increasing molar ratios of MBP or MBP-pacsin 2 SH3 domain (0.5–100 µg) for 2 h at 4°C. After washing in HNMT, bounds proteins were eluted in SDS sample buffer and analyzed by SDS–PAGE and Western blotting or Coomassie blue staining.

Lipid phosphatase assays

Lipids (1,2-dioleoyl-sn-glycero-3-phosphocholine [DOPC], 1,2-dioleoyl-sn-glycero-3-phospho-l-serine [DOPS], and natural PtdIns(4,5)P_2) were obtained from Avanti Polar Lipids (Alabaster, AL). All other chemicals were from Sigma-Aldrich and of the highest grade available. Lipid vesicles containing 60 mol% DOPC, 30 mol% DOPS, and 10 mol% natural PtdIns(4,5)P_2 were prepared by extrusion. The lipid mixture of DOPC, DOPS, and PtdIns(4,5)P_2 was dissolved in chloroform/methanol (2:1). The lipid solution was dried by evaporation under nitrogen gas. The dried lipid was then hydrated using 20 mM HEPES, pH 7.4, to a final lipid concentration of 1 mM for 1 h at room temperature. Once the lipids were fully hydrated, the lipid mixtures were extruded using polycarbonate membranes with pore sizes of 30 and 200 nm, respectively. For the activity assay, His/S-OCRL1 (30 nM) was allowed to interact with the indicated proteins on ice for 20 min in 20 mM HEPES, pH 7.4, containing 100 mM NaCl, 4 mM $MgCl_2$, and 0.5 mM dithiothreitol. The phosphatase activity was monitored as previously described (Mak et al., 2011). The phosphatase reaction

was started by addition of lipid vesicles. After incubation at 37°C for 20 min, the reaction was stopped by adding equal volumes of malachite green dye, and the resulting absorbance was read at 625 nm.

Microscopy quantitation and statistical analysis

Quantitation of colocalization was performed using the Coloc2 plug-in in ImageJ, with Pearson's *r* from 64 cells determined. The CD8-CIMPR recycling experiments were quantified by scoring the phenotypes of 50–100 cells from two or three independent experiments or by measuring the extent of colocalization between endocytosed CD8-CIMPR and golgin97 using ImageJ. For analysis of tubulation, tubules were identified as thin, elongated structures with a length at least 1.5× greater than their width, as determined by eye. Tubule lengths were recorded by tracing a line over the tubule (or the maximum tubule length for live-cell movies, for which the movie was paused at the frame in which a tubule was at its maximum length and a line was traced along it) with the Freehand line tool in ImageJ and then counted and measured using the Measure command. The average length of tubule per cell was then calculated using Excel (Microsoft, Redmond, WA). Means were compared using the one-way analysis of variance (ANOVA) test or Student's *t* test, or using a Mann–Whitney test or a Kruskal–Wallis test if data were not normally distributed, as indicated, with GraphPad Prism 6 (GraphPad Software, La Jolla, CA). The SD, SEM, and graphs were calculated or generated using GraphPad Prism 6. Adjusted *p* values calculated using Dunnett's adjustments are reported, where multiple comparisons have been conducted using one-way ANOVA. Student's *t* tests were conducted using Welch's correction to assume that samples did not have equal variances.

REFERENCES

Anitei M, Hoflack B (2011). Bridging membrane and cytoskeleton dynamics in the secretory and endocytic pathways. Nat Cell Biol 14, 11–19.

Anitei M, Stange C, Parshina I, Baust T, Schenck A, Raposo G, Kirchhausen T, Hoflack B (2010). Protein complexes containing CYFIP/Sra/PIR121 coordinate Arf1 and Rac1 signalling during clathrin-AP-1-coated carrier biogenesis at the TGN. Nat Cell Biol 12, 330–340.

Arighi CN, Hartnell LM, Aguilar RC, Haft CR, Bonifacino JS (2004). Role of the mammalian retromer in sorting of the cation-independent mannose 6-phosphate receptor. J Cell Biol 165, 123–133.

Attree O, Olivos IM, Okabe I, Bailey LC, Nelson DL, Lewis RA, McInnes RR, Nussbaum RL (1992). The Lowe's oculocerebrorenal syndrome gene encodes a protein highly homologous to inositol polyphosphate-5-phosphatase. Nature 358, 239–242.

Balla T (2013). Phosphoinositides: tiny lipids with giant impact on cell regulation. Physiol Rev 93, 1019–1137.

Ben El Kadhi K, Roubinet C, Solinet S, Emery G, Carreno S (2011). The inositol 5-phosphatase dOCRL controls PI(4,5)P2 homeostasis and is necessary for cytokinesis. Curr Biol 21, 1074–1079.

Billcliff PG, Lowe M (2014). Inositol lipid phosphatases in membrane trafficking and human disease. Biochem J 461, 159–175.

Bohdanowicz M, Balkin DM, De Camilli P, Grinstein S (2012). Recruitment of OCRL and Inpp5B to phagosomes by Rab5 and APPL1 depletes phosphoinositides and attenuates Akt signaling. Mol Biol Cell 23, 176–187.

Borner GH, Hein MY, Hirst J, Edgar JR, Mann M, Robinson MS (2014). Fractionation profiling: a fast and versatile approach for mapping vesicle proteomes and protein-protein interactions. Mol Biol Cell 25, 3178–3194.

Carlton J, Bujny M, Peter BJ, Oorschot VM, Rutherford A, Mellor H, Klumperman J, McMahon HT, Cullen PJ (2004). Sorting nexin-1 mediates tubular endosome-to-TGN transport through coincidence sensing of high-curvature membranes and 3-phosphoinositides. Curr Biol 14, 1791–1800.

Chang-Ileto B, Frere SG, Chan RB, Voronov SV, Roux A, Di Paolo G (2011). Synaptojanin 1-mediated PI(4,5)P2 hydrolysis is modulated by membrane curvature and facilitates membrane fission. Dev Cell 20, 206–218.

Choudhury R, Diao A, Zhang F, Eisenberg E, Saint-Pol A, Williams C, Konstantakopoulos A, Lucocq J, Johannes L, Rabouille C, *et al.* (2005). Lowe syndrome protein OCRL1 interacts with clathrin and regulates protein trafficking between endosomes and the trans-Golgi network. Mol Biol Cell 16, 3467–3479.

Choudhury R, Noakes CJ, McKenzie E, Kox C, Lowe M (2009). Differential clathrin binding and subcellular localization of OCRL1 splice isoforms. J Biol Chem 284, 9965–9973.

Coon BG, Hernandez V, Madhivanan K, Mukherjee D, Hanna CB, Baringa-Rementeria Ramirez I, Lowe M, Beales PL, Aguilar RC (2012). The Lowe syndrome protein OCRL1 is involved in primary cilia assembly. Hum Mol Genet 21, 1835–1847.

Coon BG, Mukherjee D, Hanna CB, Riese DJ 2nd, Lowe M, Aguilar RC (2009). Lowe syndrome patient fibroblasts display Ocrl1-specific cell migration defects that cannot be rescued by the homologous Inpp5b phosphatase. Hum Mol Genet 18, 4478–4491.

Cui S, Guerriero CJ, Szalinski CM, Kinlough CL, Hughey RP, Weisz OA (2010). OCRL1 function in renal epithelial membrane traffic. Am J Physiol Renal Physiol 298, F335–F345.

Dambournet D, Machicoane M, Chesneau L, Sachse M, Rocancourt M, El Marjou A, Formstecher E, Salomon R, Goud B, Echard A (2011). Rab35 GTPase and OCRL phosphatase remodel lipids and F-actin for successful cytokinesis. Nat Cell Biol 13, 981–988.

de Kreuk BJ, Anthony EC, Geerts D, Hordijk PL (2012). The F-BAR protein PACSIN2 regulates epidermal growth factor receptor internalization. J Biol Chem 287, 43438–43453.

de Kreuk BJ, Nethe M, Fernandez-Borja M, Anthony EC, Hensbergen PJ, Deelder AM, Plomann M, Hordijk PL (2011). The F-BAR domain protein PACSIN2 associates with Rac1 and regulates cell spreading and migration. J Cell Sci 124, 2375–2388.

Derivery E, Sousa C, Gautier JJ, Lombard B, Loew D, Gautreau A (2009). The Arp2/3 activator WASH controls the fission of endosomes through a large multiprotein complex. Dev Cell 17, 712–723.

Diao A, Rahman D, Pappin DJ, Lucocq J, Lowe M (2003). The coiled-coil membrane protein golgin-84 is a novel rab effector required for Golgi ribbon formation. J Cell Biol 160, 201–212.

Di Paolo G, De Camilli P (2006). Phosphoinositides in cell regulation and membrane dynamics. Nature 443, 651–657.

Duleh SN, Welch MD (2010). WASH and the Arp2/3 complex regulate endosome shape and trafficking. Cytoskeleton (Hoboken) 67, 193–206.

Erdmann KS, Mao Y, McCrea HJ, Zoncu R, Lee S, Paradise S, Modregger J, Biemesderfer D, Toomre D, De Camilli P (2007). A role of the Lowe syndrome protein OCRL in early steps of the endocytic pathway. Dev Cell 13, 377–390.

Giridharan SS, Cai B, Vitale N, Naslavsky N, Caplan S (2013). Cooperation of MICAL-L1, Syndapin2 and phosphatidic acid in tubular recycling endosome biogenesis. Mol Biol Cell 24, 1776–1790.

Godi A, Pertile P, Meyers R, Marra P, Di Tullio G, Iurisci C, Luini A, Corda D, De Matteis MA (1999). ARF mediates recruitment of PtdIns-4-OH kinase-beta and stimulates synthesis of PtdIns(4,5)P2 on the Golgi complex. Nat Cell Biol 1, 280–287.

Gomez TS, Billadeau DD (2009). A FAM21-containing WASH complex regulates retromer-dependent sorting. Dev Cell 17, 699–711.

Grieve AG, Daniels RD, Sanchez-Heras E, Hayes MJ, Moss SE, Matter K, Lowe M, Levine TP (2011). Lowe syndrome protein OCRL1 supports maturation of polarized epithelial cells. PLoS One 6, e24044.

Hansen CG, Howard G, Nichols BJ (2011). Pacsin 2 is recruited to caveolae and functions in caveolar biogenesis. J Cell Sci 124, 2777–2785.

Harterink M, Port F, Lorenowicz MJ, McGough IJ, Silhankova M, Betist MC, van Weering JR, van Heesbeen RG, Middelkoop TC, Basler K, et al. (2011). A SNX3-dependent retromer pathway mediates retrograde transport of the Wnt sorting receptor Wntless and is required for Wnt secretion. Nat Cell Biol 13, 914–923.

Hirst J, Borner GH, Antrobus R, Peden AA, Hodson NA, Sahlender DA, Robinson MS (2012). Distinct and overlapping roles for AP-1 and GGAs revealed by the "knocksideways" system. Curr Biol 22, 1711–1716.

Hoopes RR Jr, Shrimpton AE, Knohl SJ, Hueber P, Hoppe B, Matyus J, Simckes A, Tasic V, Toenshoff B, Suchy SF, et al. (2005). Dent disease with mutations in OCRL1. Am J Hum Genet 76, 260–267.

Hou X, Hagemann N, Schoebel S, Blankenfeldt W, Goody RS, Erdmann KS, Itzen A (2011). A structural basis for Lowe syndrome caused by mutations in the Rab-binding domain of OCRL1. EMBO J 30, 1659–1670.

Hyvola N, Diao A, McKenzie E, Skippen A, Cockcroft S, Lowe M (2006). Membrane targeting and activation of the Lowe syndrome protein OCRL1 by rab GTPases. EMBO J 25, 3750–3761.

Kessels MM, Dong J, Leibig W, Westermann P, Qualmann B (2006). Complexes of syndapin II with dynamin II promote vesicle formation at the trans-Golgi network. J Cell Sci 119, 1504–1516.

Kessels MM, Qualmann B (2004). The syndapin protein family: linking membrane trafficking with the cytoskeleton. J Cell Sci 117, 3077–3086.

Kostan J, Salzer U, Orlova A, Toro I, Hodnik V, Senju Y, Zou J, Schreiner C, Steiner J, Merilainen J, et al. (2014). Direct interaction of actin filaments with F-BAR protein pacsin2. EMBO Rep 15, 1154–1162.

Kuhbacher A, Dambournet D, Echard A, Cossart P, Pizarro-Cerda J (2012). Phosphatidylinositol 5-phosphatase oculocerebrorenal syndrome of Lowe protein (OCRL) controls actin dynamics during early steps of Listeria monocytogenes infection. J Biol Chem 287, 13128–13136.

Luo N, West CC, Murga-Zamalloa CA, Sun L, Anderson RM, Wells CD, Weinreb RN, Travers JB, Khanna H, Sun Y (2012). OCRL localizes to the primary cilium: a new role for cilia in Lowe syndrome. Hum Mol Genet 21, 3333–3344.

Mak LH, Vilar R, Woscholski R (2011). Characterisation of the PTEN inhibitor VO-OHpic. J Chem Biol 3, 157–163.

Marion S, Mazzolini J, Herit F, Bourdoncle P, Kambou-Pene N, Hailfinger S, Sachse M, Ruland J, Benmerah A, Echard A, et al. (2012). The NF-kappaB signaling protein Bcl10 regulates actin dynamics by controlling AP1 and OCRL-bearing vesicles. Dev Cell 23, 954–967.

Maxfield FR, McGraw TE (2004). Endocytic recycling. Nat Rev Mol Cell Biol 5, 121–132.

McCrea HJ, De Camilli P (2009). Mutations in phosphoinositide metabolizing enzymes and human disease. Physiology (Bethesda) 24, 8–16.

McMahon HT, Boucrot E (2011). Molecular mechanism and physiological functions of clathrin-mediated endocytosis. Nat Rev Mol Cell Biol 12, 517–533.

Mehta ZB, Pietka G, Lowe M (2014). The cellular and physiological functions of the Lowe syndrome protein OCRL1. Traffic 15, 471–487.

Miki H, Miura K, Takenawa T (1996). N-WASP, a novel actin-depolymerizing protein, regulates the cortical cytoskeletal rearrangement in a PIP2-dependent manner downstream of tyrosine kinases. EMBO J 15, 5326–5335.

Nandez R, Balkin DM, Messa M, Liang L, Paradise S, Czapla H, Hein MY, Duncan JS, Mann M, De Camilli P (2014). A role of OCRL in clathrin-coated pit dynamics and uncoating revealed by studies of Lowe syndrome cells. Elife 3, e02975.

Noakes CJ, Lee G, Lowe M (2011). The PH domain proteins IPIP27A and B link OCRL1 to receptor recycling in the endocytic pathway. Mol Biol Cell 22, 606–623.

Pirruccello M, De Camilli P (2012). Inositol 5-phosphatases: insights from the Lowe syndrome protein OCRL. Trends Biochem Sci 37, 134–143.

Pirruccello M, Swan LE, Folta-Stogniew E, De Camilli P (2011). Recognition of the F&H motif by the Lowe syndrome protein OCRL. Nat Struct Mol Biol 18, 789–795.

Qualmann B, Koch D, Kessels MM (2011). Let's go bananas: revisiting the endocytic BAR code. EMBO J 30, 3501–3515.

Quan A, Robinson PJ (2014). Syndapin—a membrane remodelling and endocytic F-BAR protein. FEBS J 280, 5198–5212.

Rao Y, Ma Q, Vahedi-Faridi A, Sundborger A, Pechstein A, Puchkov D, Luo L, Shupliakov O, Saenger W, Haucke V (2010). Molecular basis for SH3 domain regulation of F-BAR-mediated membrane deformation. Proc Natl Acad Sci USA 107, 8213–8218.

Rbaibi Y, Cui S, Mo D, Carattino M, Rohatgi R, Satlin LM, Szalinski CM, Swanhart LM, Folsch H, Hukriede NA, Weisz OA (2012). OCRL1 modulates cilia length in renal epithelial cells. Traffic 13, 1295–1305.

Santiago-Tirado FH, Bretscher A (2011). Membrane-trafficking sorting hubs: cooperation between PI4P and small GTPases at the trans-Golgi network. Trends Cell Biol 21, 515–525.

Sasaki T, Takasuga S, Sasaki J, Kofuji S, Eguchi S, Yamazaki M, Suzuki A (2009). Mammalian phosphoinositide kinases and phosphatases. Prog Lipid Res 48, 307–343.

Seaman MN (2004). Cargo-selective endosomal sorting for retrieval to the Golgi requires retromer. J Cell Biol 165, 111–122.

Senju Y, Itoh Y, Takano K, Hamada S, Suetsugu S (2011). Essential role of PACSIN2/syndapin-II in caveolae membrane sculpting. J Cell Sci 124, 2032–2040.

Shi A, Liu O, Koenig S, Banerjee R, Chen CC, Eimer S, Grant BD (2012). RAB-10-GTPase-mediated regulation of endosomal phosphatidylinositol-4,5-bisphosphate. Proc Natl Acad Sci USA 109, E2306–E2315.

Shimada A, Takano K, Shirouzu M, Hanawa-Suetsugu K, Terada T, Toyooka K, Umehara T, Yamamoto M, Yokoyama S, Suetsugu S (2010). Mapping of the basic amino-acid residues responsible for tubulation and cellular protrusion by the EFC/F-BAR domain of pacsin2/Syndapin II. FEBS Lett 584, 1111–1118.

Smith CM, Chircop M (2012). Clathrin-mediated endocytic proteins are involved in regulating mitotic progression and completion. Traffic 13, 1628–1641.

Suchy SF, Nussbaum RL (2002). The deficiency of PIP2 5-phosphatase in Lowe syndrome affects actin polymerization. Am J Hum Genet 71, 1420–1427.

Sun Y, Hedman AC, Tan X, Schill NJ, Anderson RA (2013). Endosomal type Igamma PIP 5-kinase controls EGF receptor lysosomal sorting. Dev Cell 25, 144–155.

Swan LE, Tomasini L, Pirruccello M, Lunardi J, De Camilli P (2010). Two closely related endocytic proteins that share a common OCRL-binding motif with APPL1. Proc Natl Acad Sci USA 107, 3511–3516.

Takeda T, Robinson IM, Savoian MM, Griffiths JR, Whetton AD, McMahon HT, Glover DM (2013). Drosophila F-BAR protein Syndapin contributes to coupling the plasma membrane and contractile ring in cytokinesis. Open Biol 3, 130081.

Taylor MJ, Perrais D, Merrifield CJ (2011). A high precision survey of the molecular dynamics of mammalian clathrin-mediated endocytosis. PLoS Biol 9, e1000604.

Temkin P, Lauffer B, Jager S, Cimermancic P, Krogan NJ, von Zastrow M (2011). SNX27 mediates retromer tubule entry and endosome-to-plasma membrane trafficking of signalling receptors. Nat Cell Biol 13, 715–721.

Ungewickell AJ, Majerus PW (1999). Increased levels of plasma lysosomal enzymes in patients with Lowe syndrome. Proc Natl Acad Sci USA 96, 13342–13344.

van Rahden VA, Brand K, Najm J, Heeren J, Pfeffer SR, Braulke T, Kutsche K (2012). The 5-phosphatase OCRL mediates retrograde transport of the mannose 6-phosphate receptor by regulating a Rac1-cofilin signalling module. Hum Mol Genet 21, 5019–5038.

Vicinanza M, D'Angelo G, Di Campli A, De Matteis MA (2008). Phosphoinositides as regulators of membrane trafficking in health and disease. Cell Mol Life Sci 65, 2833–2841.

Vicinanza M, Di Campli A, Polishchuk E, Santoro M, Di Tullio G, Godi A, Levtchenko E, De Leo MG, Polishchuk R, Sandoval L, et al. (2011). OCRL controls trafficking through early endosomes via PtdIns4,5P(2)-dependent regulation of endosomal actin. EMBO J 30, 4970–4985.

Waguri S, Dewitte F, Le Borgne R, Rouille Y, Uchiyama Y, Dubremetz JF, Hoflack B (2003). Visualization of TGN to endosome trafficking through fluorescently labeled MPR and AP-1 in living cells. Mol Biol Cell 14, 142–155.

Watt SA, Kular G, Fleming IN, Downes CP, Lucocq JM (2002). Subcellular localization of phosphatidylinositol 4,5-bisphosphate using the pleckstrin homology domain of phospholipase C delta1. Biochem J 363, 657–666.